SANDIA REPORT
SAND2009-0291
Unlimited Release
Printed January 2009

Control of Pore Size in Epoxy Systems

James Bahr, Mathias C. Celina, Bret J. Chisholm, Shawn M. Dirk, Nathan Gubbins, Alekhya Kallam, Robert J. Klein, Elizabeth Lee, Joseph L. Lenhart, Partha Majumdar, and Patricia S. Sawyer

Prepared by
Sandia National Laboratories
Albuquerque, New Mexico 87185 and Livermore, California 94550

Sandia is a multiprogram laboratory operated by Sandia Corporation,
a Lockheed Martin Company, for the United States Department of Energy's
National Nuclear Security Administration under Contract DE-AC04-94AL85000.

Approved for public release; further dissemination unlimited.

Sandia National Laboratories

Issued by Sandia National Laboratories, operated for the United States Department of Energy by Sandia Corporation.

NOTICE: This report was prepared as an account of work sponsored by an agency of the United States Government. Neither the United States Government, nor any agency thereof, nor any of their employees, nor any of their contractors, subcontractors, or their employees, make any warranty, express or implied, or assume any legal liability or responsibility for the accuracy, completeness, or usefulness of any information, apparatus, product, or process disclosed, or represent that its use would not infringe privately owned rights. Reference herein to any specific commercial product, process, or service by trade name, trademark, manufacturer, or otherwise, does not necessarily constitute or imply its endorsement, recommendation, or favoring by the United States Government, any agency thereof, or any of their contractors or subcontractors. The views and opinions expressed herein do not necessarily state or reflect those of the United States Government, any agency thereof, or any of their contractors.

Printed in the United States of America. This report has been reproduced directly from the best available copy.

Available to DOE and DOE contractors from
U.S. Department of Energy
Office of Scientific and Technical Information
P.O. Box 62
Oak Ridge, TN 37831

Telephone: (865) 576-8401
Facsimile: (865) 576-5728
E-Mail: reports@adonis.osti.gov
Online ordering: http://www.osti.gov/bridge

Available to the public from
U.S. Department of Commerce
National Technical Information Service
5285 Port Royal Rd.
Springfield, VA 22161

Telephone: (800) 553-6847
Facsimile: (703) 605-6900
E-Mail: orders@ntis.fedworld.gov
Online order: http://www.ntis.gov/help/ordermethods.asp?loc=7-4-0#online

SAND2009-0291
Unlimited Release
Printed January 2009

Control of Pore Size in Epoxy Systems

James Bahr,[1] Mathew C. Celina,[2] Bret J. Chisholm,[1,3] Shawn M. Dirk,[2] Nathan Gubbins,1 Alekhya Kallam,[1] Robert J. Klein,[2] Elizabeth Lee,[1] Joseph L. Lenhart,[1] Partha Majumdar,[1] and Patricia S. Sawyer[2]

[1]Center for Nanoscale Science and Engineering,
North Dakota State University
Fargo, North Dakota 58102

[2]Organic Materials Department,
Sandia National Laboratories, P.O. Box 5800
Albuquerque, New Mexico 87185-MS0888

[3]Department of Coatings and Polymeric Materials,
North Dakota State University
Fargo, North Dakota 58102

Abstract

Both conventional and combinatorial approaches were used to study the pore formation process in epoxy based polymer systems. Sandia National Laboratories conducted the initial work and collaborated with North Dakota State University (NDSU) using a combinatorial research approach to produce a library of novel monomers and crosslinkers capable of forming porous polymers. The library was screened to determine the physical factors that control porosity, such as porogen loading, polymer-porogen interactions, and polymer crosslink density. We have identified the physical and chemical factors that control the average porosity, pore size, and pore size distribution within epoxy based systems.

CONTENTS

1. Porous epoxies by phase separation of removable alcohols: control of spherical pore size by mass fraction, cure temperature, and reaction rate 9
1.1. Introduction 9
1.2. Experimental 10
1.1.1. Materials 10
1.1.2. Sample Preparation 11
1.1.3. Characterization and Image Analysis 11
1.3. Results and Discussion 11
1.4. Summary 17
1.5. Acknowledgements 18
1.6. References 18

2. The Development of a Combinatorial/High-Throughput Workflow for the Study of Porous Polymer Networks 21
2.1. Introduction 21
2.2. Experimental 23
2.2.1. Materials 23
2.2.2. Instrumentation 25
2.3. Results and Discussion 25
2.3.1. Description of the High-throughput/Combinatorial Workflow Developed 25
2.3.2. Porous Epoxy Networks Produced Using CIPS 27
2.4. Conclusions and Future Work 37
2.5. References 38

Distribution 41

FIGURES

Figure 1. Structures of the BADGE (epoxide), D230 (amine crosslinker), low-molecular weight filler 1-octadecanol, and catalyst 1-methylimidazole. For the amine used here, the average molecular weight is 230 g/mol, which equates to $2 < n_{avg} < 3$. 10
Figure 2. Epoxies cured at 90 ^{o}C with (a) 30 wt% octadecanol; (b) 40 wt % octadecanol; and (c) 50 wt% octadecanol. (d) epoxy cured at 75 ^{o}C with 40 wt% octadecanol. Arrows indicate the location of small pores. 12
Figure 3. Schematic of a nucleophilic imidazole derivative facilitating the cure of an epoxy and amine. The imidazole opens the epoxy ring, generating a positive charge shared between the imidazole nitrogen and the adjacent epoxy carbon, which then adds to the amine. The imidazole is then regenerated to catalyze other epoxy-amine additions. 13
Figure 4. Fracture surfaces of epoxies cured at 90 ^{o}C with 40 wt% octadecanol: (a) 0.3 wt% imidazole; (b) 0.4 wt% imidazole; and (c) 0.5 wt% imidazole. In (c), the smearing in the midsection is due to charging. 14
Figure 5. Fracture surfaces of epoxies cured at 90 ^{o}C with 40 wt% octadecanol: (a) 0.6 wt% imidazole; (b) 0.8 wt% imidazole; and (c) 0.9 wt% imidazole. Arrows indicate the location of

small pores. In the high-magni_cation image of (c), the "cracks" are actually due to the gold-palladium coating, and not related to the polymer fracture surface. 15
Figure 6. Pore diameter *d*, volume fraction, and gel time as a function of the amount of imidazole added relative to the amount of epoxy. All data represent a curing temperature of 90 ^{o}C and 40 wt% imidazole. The dashed line is the best linear fit to the gel times. If not shown, estimated errors are ±10 %. 16
Figure 7. Representative phase diagrams showing UCST behavior (left) and LCST behavior (right). 22
Figure 8. A schematic illustration describing morphology development associated with spinodal decomposition. 22
Figure 9. A schematic illustration of the high-throughput workflow that was developed. 26
Figure 10. An image of the robotic system used for preparing liquid blends. 26
Figure 11. An image of the boring device used to extract cylindrical specimens of cured material (left) and the device used for preparing sample discs from the cylindrical specimen (right). 27
Figure 12. An image of the device used for poragen extraction of an array of 64 samples. 27
Figure 13. A schematic illustrating the formation of the crosslinked network. 28
Figure 14. A schematic illustration of the experimental design used for the study. 30
Figure 15. Tg as a function of crosslinker equivalent weight (g/mole NH_2) for the cured polymer networks (no poragen). 31
Figure 16. SEM images of fracture surfaces obtained from cured polymer networks (no poragen). 31
Figure 17. Images illustrating the various types of phase behavior exhibited by blends at room temperature. 33
Figure 18. Phase behavior of uncured blends at room temperature and fully cured blends as a function of poragen solubility parameter. 34
Figure 19. Representative images of fracture surfaces for 24 different samples. 35
Figure 20. SEM images of fracture surfaces of materials based on Hxl as the crosslinker and cured at 40 °C. 36
Figure 21. SEM images of fracture surfaces of materials based on MCHA as the crosslinker and cured at 40 °C. 36
Figure 22. A schematic of the gradient plate design. 38

TABLES

Table 1. A description of the starting materials used for the study. 23
Table 2. Composition of the each of the blends prepared. All weights are in grams. 23
Table 3. Solubility parameters for poragens, polymer network-forming precursors, and polymer network. 28
Table 4. Results of observations made at room temperature regarding blend miscibility. "+" indicates the formation of a miscible blend while "-" indicates the formation of a two-phase blend..... 32
Table 5. Results of visual observations made regarding the phase behavior of the cured materials. "T" indicates the observation shown in Figure 11a, "O" indicates the observation shown in Figure 11b, and "2L" indicates the observation shown in Figure 11c. 34

NOMENCLATURE

DOE	Department of Energy
CIPS	Chemically induced phase separation
TIPS	Thermally induced phase separation
SD	spinodal decomposition
NG	nucleation and growth
MCHA	4,4'-methyl bis(cyclohexylamine)
UCST	upper critical solution temperature
LCST	lower critical solution temperature
SEM	scanning electron microscope
BET	Brunauer, Emmett and Teller
Ep	Bisphenol –A- diglycidylether
Lxl	Amino-terminated polypropylene glycol with molecular weight 230 g/mol
Mxl	Amino-terminated polypropylene glycol with molecular weight 430 g/mol
Hxl	Amino-terminated polypropylene glycol with molecular weight 2000 g/mol
MCHA	4,4'-methylenebis(cyclohexylamine)
De	Decane
Dol	n-Decanol
PMA	Propylene glycol methyl ether acetate
EEP	Ethyl-3-ethoxy propionate
MAK	2-Heptanone
DBK	2,6-Dimethyl-4-heptanone
SNL	Sandia National Laboratories

1. POROUS EPOXIES BY PHASE SEPARATION OF REMOVABLE ALCOHOLS: CONTROL OF SPHERICAL PORE SIZE BY MASS FRACTION, CURE TEMPERATURE, AND REACTION RATE

1.1. Introduction

Precise control of porosity on the micron to nanometer scale is critically important to many polymer applications. Recent examples of applications utilizing porosity for improved properties are silica aerogels [1], chemical sensors [2,3,4], battery electrolytes and electrodes [5,6,7], hydrogen storage materials [8,9], tissue scaffolds [10,11], and low-dielectric constant materials for electronic packaging [12]. Porosity may lead to beneficial effects on mechanical or electrical properties, permeability, or adsorption and desorption of gases or liquids [13]. Critically important is the impact of porosity on the two physical properties of density and surface area.

There are two fundamental routes to porosity in polymers: blowing due to sudden gas expansion (as with polymer foams) and the removal of one or more sacrificial phases. This paper utilizes the latter, which encompasses such diverse preparation techniques as the use of water-soluble salt crystals or acid-soluble silica spheres [14,15], phase separating block copolymers where one phase can be preferentially hydrolyzed [16,13], semi-crystalline polymers gelling from solvent that are then carbonized [17], and inverse or bicontinuous microemulsions [18,19,20]. Here we will be focusing on reaction-induced phase-decomposition (also called chemically-induced phase separation, or CIPS), excellently described by Inoue et al.[21,22] and Williams et al.[23]. CIPS, which proceeds over time as a result of chemical reactions, is similar to the well-established thermally-induced phase separation (TIPS), which involves manipulating temperature to lead to various morphologies. TIPS has been exploited in many different systems [24], although perhaps the clearest example is that of block copolymers [25], where the $\chi N(x)$ phase diagram may contain eight or more distinct phases. The χ parameter is that introduced by the Flory-Huggins relation, N is the degree of polymerization, and x is the composition. Also critical in the TIPS of block copolymers is the distinction between spinodal decomposition (SD) or nucleation and growth (NG), where the former is induced by a sudden large change in temperature or composition and leads to a bicontinuous network, and the latter is induced by slow changes and leads to spherical inclusions in a continuous matrix [25]. In CIPS, both SD and NG are accessible [22,26,23,27], and selection between these two routes depends on three factors: phase separation rate (driven by thermodynamics), reaction rate, and chain mobility (rate of interdiffusion). In general, as the ratio of phase separation rate to reaction rate increases, NG is more likely; and as chain mobility decreases relative to phase separation rate, SD is more likely. Therefore the phase separation mechanism may be viewed as a balance between the rate separate phases form to the rate that they are frozen in place.

The present paper utilizes a mixture of an epoxide, an amine, and an unreactive alcohol to produce spherical voids in an epoxy matrix, after removal of the alcohol. The advantages of the present technique over other methods are several-fold. First, the chemistry is limited to only three or four inexpensive chemicals, all of which are relatively stable to water and oxygen, relatively non-toxic, and very forgiving to alterations of the preparation method. Methods such as bicontinuous microemulsions or spinodal decomposition of block copolymers, which have the

benefit of producing open pore structures that are in some cases better for membrane applications, involve expensive starting materials (tailored block copolymers) or complex formulations (oils, water, polymer starting materials, and interfacial agents [19]). Second, the pore size produced by the present CIPS method can be easily adjusted by changing reaction rate (by temperature or catalyst concentration) or concentration of unreactive alcohol, to produce spherical pores ranging from ~50 µm to ~10 nm. Third, the epoxy and amine used in this study are available in a wide range of molecular weights (by modifying the spacer length between reactive endgroups), and the spacer chemistry (propylene glycol in the current study) of the spacers can be easily exchanged to induce significant changes in the mechanical and electrical properties of the final epoxy.

Ultimately, the purpose of this paper is to highlight a simple mechanism to control pore size (µm to tens of nm) and pore volume fraction (high to low) by controlling reaction kinetics and phase behavior in a crosslinking system.

1.2. Experimental

1.1.1. Materials

All samples utilized the same di-functional epoxide mixed in stoichiometric proportions with a tetra-functional amine. The epoxide was glycidyl end-capped poly(bisphenol A-co-epichlorohydrin) (BADGE), with average molecular weight 345 g/mol, obtained from Sigma-Aldrich. The amine was poly(oxypropylene)diamine (D230), a jeffamine, with average molecular weight 230 g/mol, obtained from Sigma-Aldrich. Structures of the BADGE and D230 are shown in Figure 1.

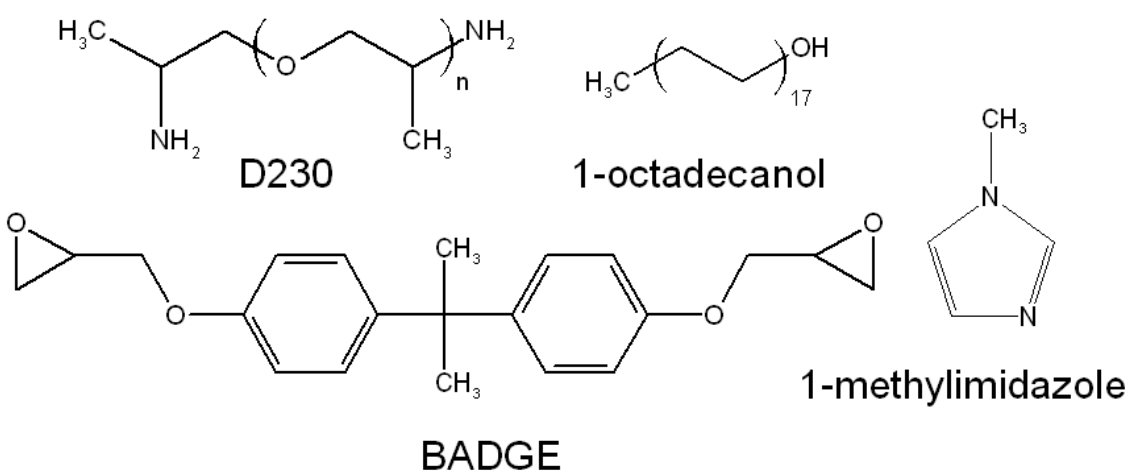

Figure 1. Structures of the BADGE (epoxide), D230 (amine crosslinker), low-molecular weight filler 1-octadecanol, and catalyst 1-methylimidazole. For the amine used here, the average molecular weight is 230 g/mol, which equates to $2 < n_{avg} < 3$.

1-octadecanol (95 %) was obtained from Fisher Scientific. 1-methylimidazole (99+ %), under the trade name IMICURE AMI-1 curing agent, was obtained from Air Products and Chemicals. The

density of the epoxide, amine, and octadecanol are 1.160, 0.9702, and 0.8120 g/cm^3, respectively, meaning that a sample designated 40 wt% octadecanol contains 48 vol%.

1.1.2. Sample Preparation

The epoxide and amine were mixed in stoichiometric proportions with a mechanical mixer for 5 min at 1500 rpm. The octadecanol was melted in an 80-90 ^{o}C oven in predetermined masses, the epoxy liquid was pre-heated to 90 ^{o}C, and the two liquids were mixed at ~90 ^{o}C for 2 min at 1200 rpm. If needed, methylimidazole was measured (via a micro-pipette) and added immediately prior to the final mixing stage. Samples were cured for 15 h at the specified temperatures. They were then fractured at 0 ^{o}C, and the octadecanol was removed under a 125 ^{o}C vacuum for 17 h.

1.1.3. Characterization and Image Analysis

Images were taken with a Zeiss Supra55VP, field emission gun, scanning electron microscope. Samples were coated with a gold-palladium mixture and imaged with 5 kV accelerating voltage, in high vacuum mode. For most samples a secondary electron detector was used (working distance 15 mm), but in surfaces where pores were very small or not present (pore diameter $<$ 50 nm), a shorter working distance (5 mm) and the in-lens detector were used.

Volume fractions of pores V_p were estimated using the rule of classical stereology that $V_V = P_P$, or that the average volume fraction of the species of interest is equal to the average proportion of test points that are covered by the species of interest [28]. 230 points on a grid were visually assessed to obtain P_P and thus the volume fraction of pores. An assumption was made that the fracture surface is flat, rather than three-dimensional, and the inaccuracy of this probably overestimates the pore volume fraction slightly, especially for a higher volume fraction of pores. However, the measured V_p never exceeds the maximum V_p of 48 vol%, so the overestimation is not unphysical.

Gel time is approximated as the time during the curing process at which a sharp increase in viscosity occurs that accompanies long-range network formation. Relative changes in viscosity are measured qualitatively using a stainless steel probe inserted into the mixture through a port in the curing oven, and the probe was stirred through the mixture every 30 s and the response observed visually.

1.3. Results and Discussion

Composition plays a critical role in phase separation of this system. As composition increases from 30 wt% to 50 wt% octadecanol at a cure temperature of 90 ^{o}C, the pores in Figure 2 increase from barely visible with the SEM (diameters on the order of 10 nm) to extremely large (~3 μm). To the naked eye, the 30 wt% sample is optically transparent whereas samples with higher octadecanol fraction are opaque and appear white.

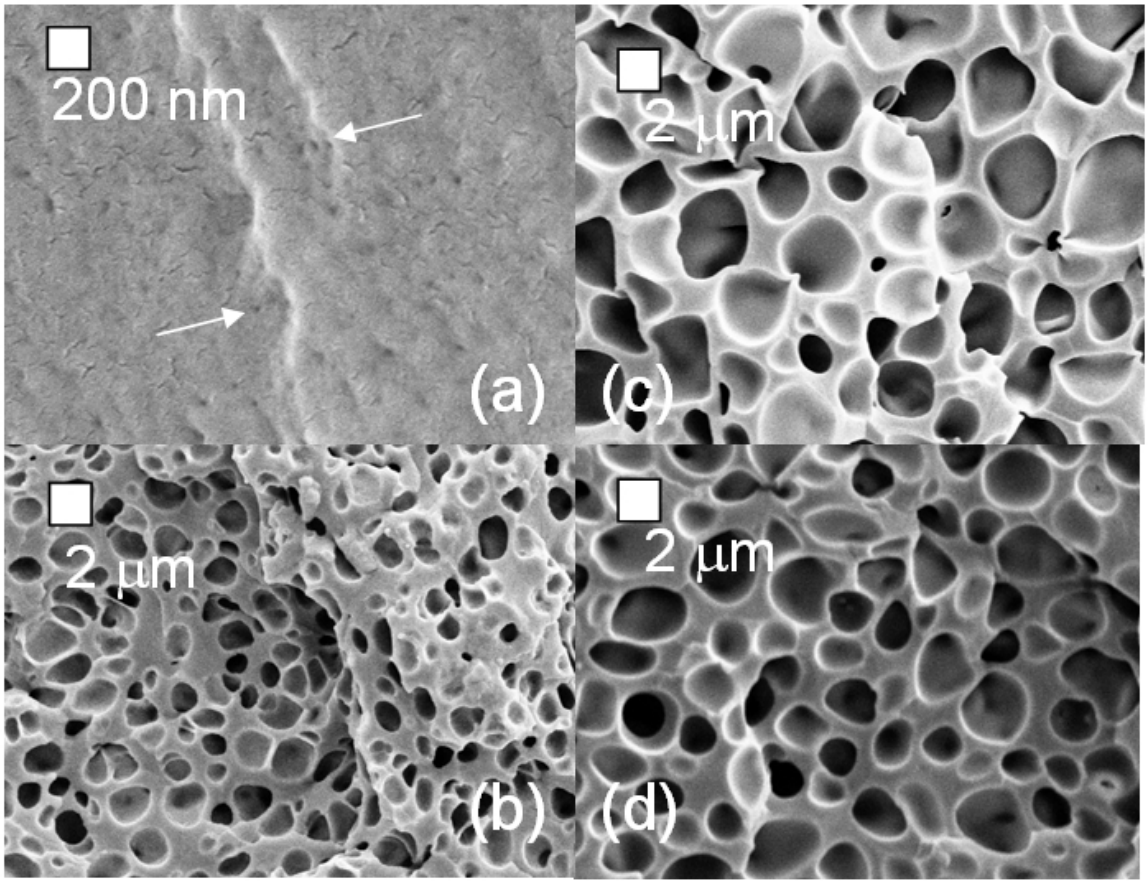

Figure 2. Epoxies cured at 90 ^{o}C with (a) 30 wt% octadecanol; (b) 40 wt % octadecanol; and (c) 50 wt% octadecanol. (d) epoxy cured at 75 ^{o}C with 40 wt% octadecanol. Arrows indicate the location of small pores.

Cure temperature is also an important variable, and delineates in rough terms the impact of cure rate. As cure temperature decreases from 90 to 75 ^{o}C (micrograph (d) versus (b) in Figure 2), pore diameter increases by a factor of ~2. It is hard to distinguish between the effects of thermodynamic miscibility and kinetically-driven gel point as the temperature is lowered, but based on observations of cloud points in these mixtures, temperature has a minor effect on miscibility. (Samples were visually inspected during the curing process, and for a large range of temperatures samples remained clear, as long as the octadecanol did not crystallize.) Therefore the increase in pore diameter as temperature decreases is likely primarily due to longer time allowed for growth of the spherical inclusions in the matrix before the gel point is reached.

The addition of methylimidazole as a catalyst can increase the cure rate substantially. The imidazole was systematically used to “quench" pores at early stages of growth, prior to extensive growth of octadecanol inclusions. The fraction of imidazole is sufficiently small in the mixtures here that it will not lead to significant shifts in composition on a thermodynamic phase diagram, so changes observed in morphology must arise from kinetically arresting the process of phase separation. While nucleophilic catalysis using imidazole derivatives in epoxy-anhydride resin systems is mechanistically easily explained via ring-opening catalysis [29,30], it is more challenging to establish how nucleophilic catalysis accelerates the epoxy amine addition reaction. Imidazole likely catalyzes the amine-epoxide reaction by assisting the nucleophilic

addition of the amine. This may occur via an intermediate imidazole-epoxy adduct, where after ring opening the approaching amine substitutes the imidazole on the epoxy carbon as shown in Figure 3. The net result is an accelerated epoxy-amine cure. The precise mechanism is unclear but there is a definite increased cure rate in the presence of the imidazole. Figures 4 and 5 denote the dramatic changes observed in the morphology as the cure rate increases: pore diameters decrease from microns to tens of nanometers until, at a critical fraction of imidazole, pores are no longer visible by SEM. All samples with imidazole mass fraction greater than 0.9 wt% (not shown here) exhibited no visible pores, similar to Figure 5(c), although the texture of the fracture surface contains much fewer ridges and topological features for the higher imidazole mass fractions. This suggests that even with no visible pores in micrograph (c), there may still be stress concentrators in the form of nucleated pores that lead to a rough surface. It should be noted that the interaction between the two concurrent processes, curing and the phase separation, may impact the molecular structure of the crosslinked network (dangling ends, loops, etc.), therefore also affecting the fracture surface.

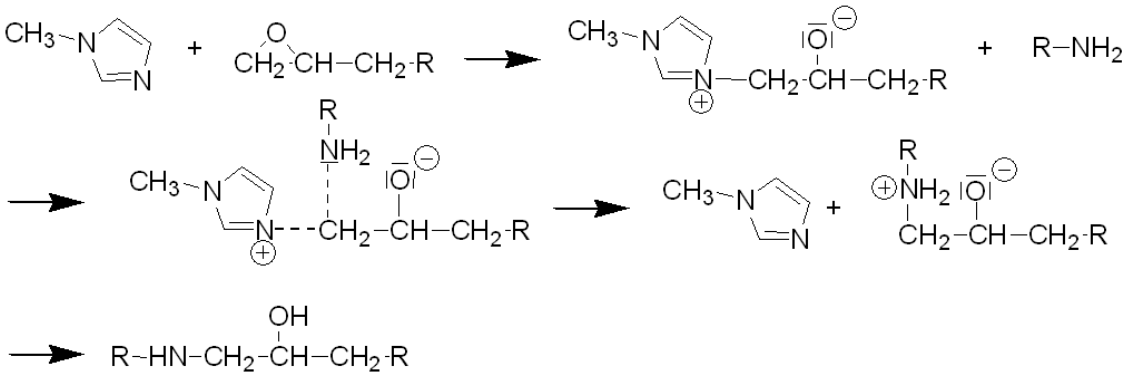

Figure 3. Schematic of a nucleophilic imidazole derivative facilitating the cure of an epoxy and amine. The imidazole opens the epoxy ring, generating a positive charge shared between the imidazole nitrogen and the adjacent epoxy carbon, which then adds to the amine. The imidazole is then regenerated to catalyze other epoxy-amine additions.

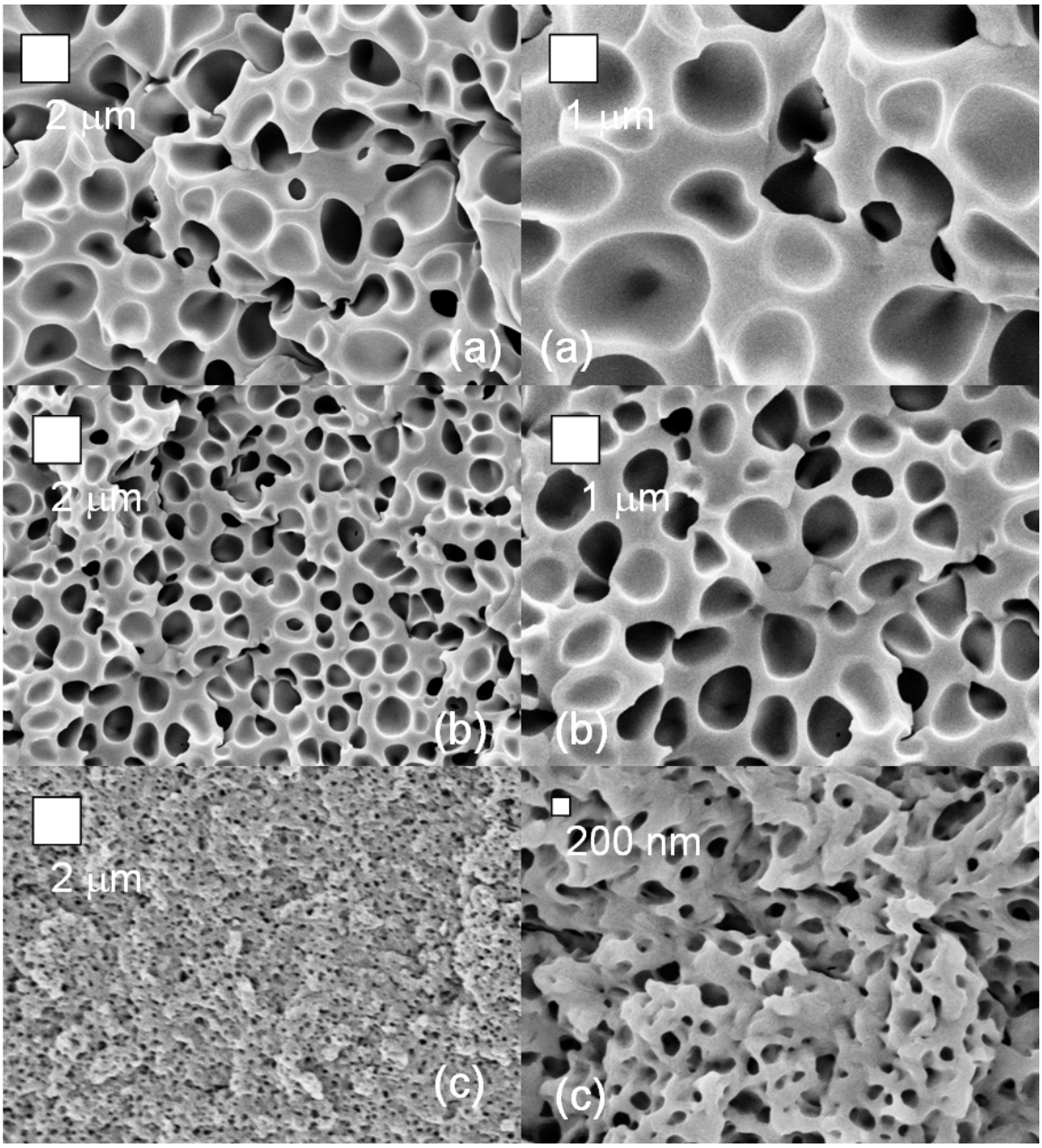

Figure 4. Fracture surfaces of epoxies cured at 90 ^{o}C with 40 wt% octadecanol: (a) 0.3 wt% imidazole; (b) 0.4 wt% imidazole; and (c) 0.5 wt% imidazole. In (c), the smearing in the midsection is due to charging.

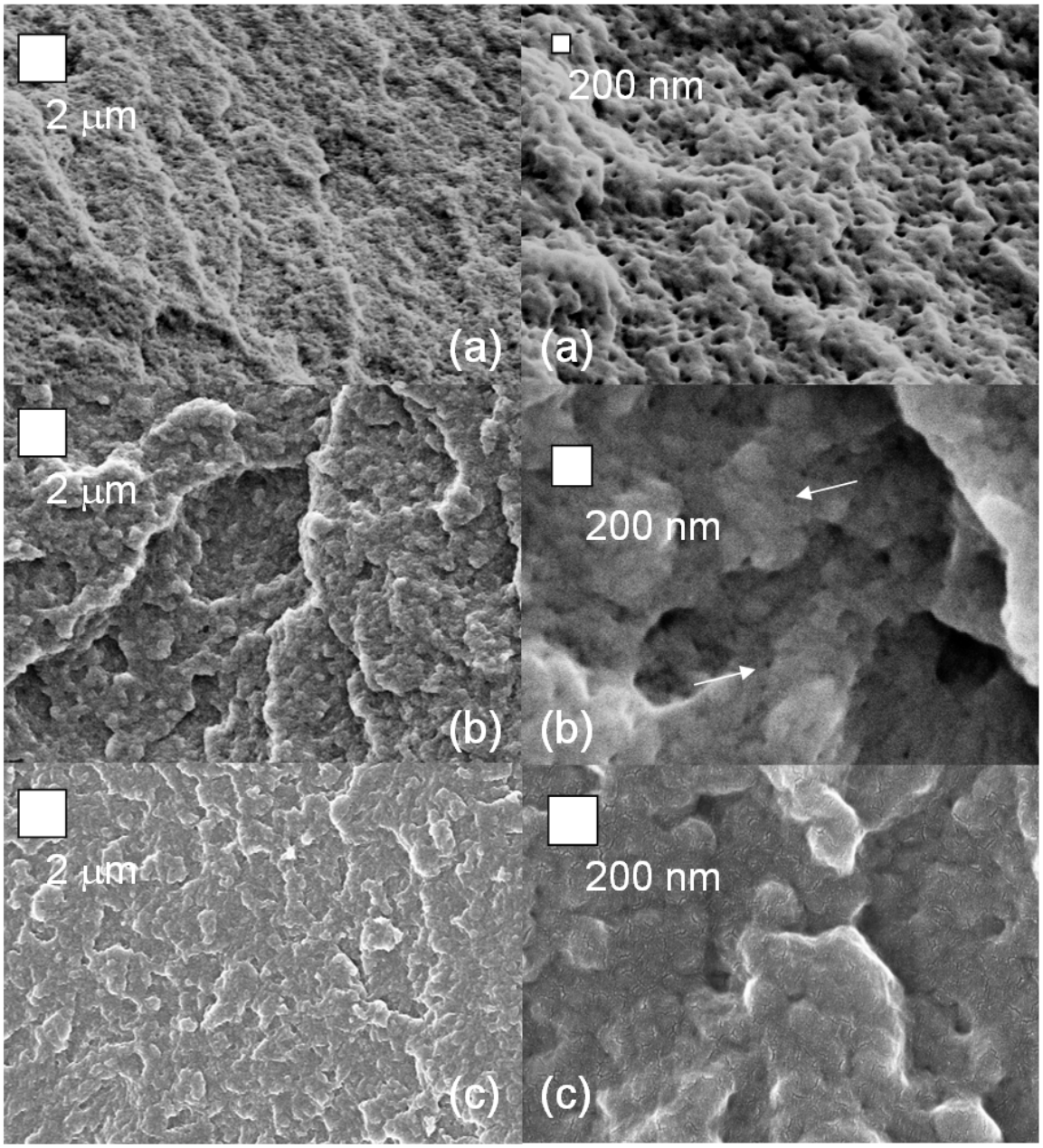

Figure 5. Fracture surfaces of epoxies cured at 90 ^{o}C with 40 wt% octadecanol: (a) 0.6 wt% imidazole; (b) 0.8 wt% imidazole; and (c) 0.9 wt% imidazole. Arrows indicate the location of small pores. In the high-magni_cation image of (c), the "cracks" are actually due to the gold-palladium coating, and not related to the polymer fracture surface.

Data gleaned from the SEM micrographs, for varying imidazole fraction at 40 wt% octadecanol and 90 ^{o}C, are plotted in Figure 6. This plot includes the characteristic parameters of pore diameter, pore volume fraction, and gel time. The key point is that pore size is tunable across three orders of magnitude with a very simple change to the formulation, via the addition of catalyst to increase the reaction rate. Gel time decreases linearly with the addition of imidazole. A sizeable drawback to the method, however, is represented by the decrease in pore volume fraction: since the kinetics lead to the decreases in pore diameter rather than thermodynamics,

there can be substantial amounts of the sacrificial phase temporarily trapped into the matrix as the cure rate becomes very high, leading to a simultaneous decrease in pore volume fraction.

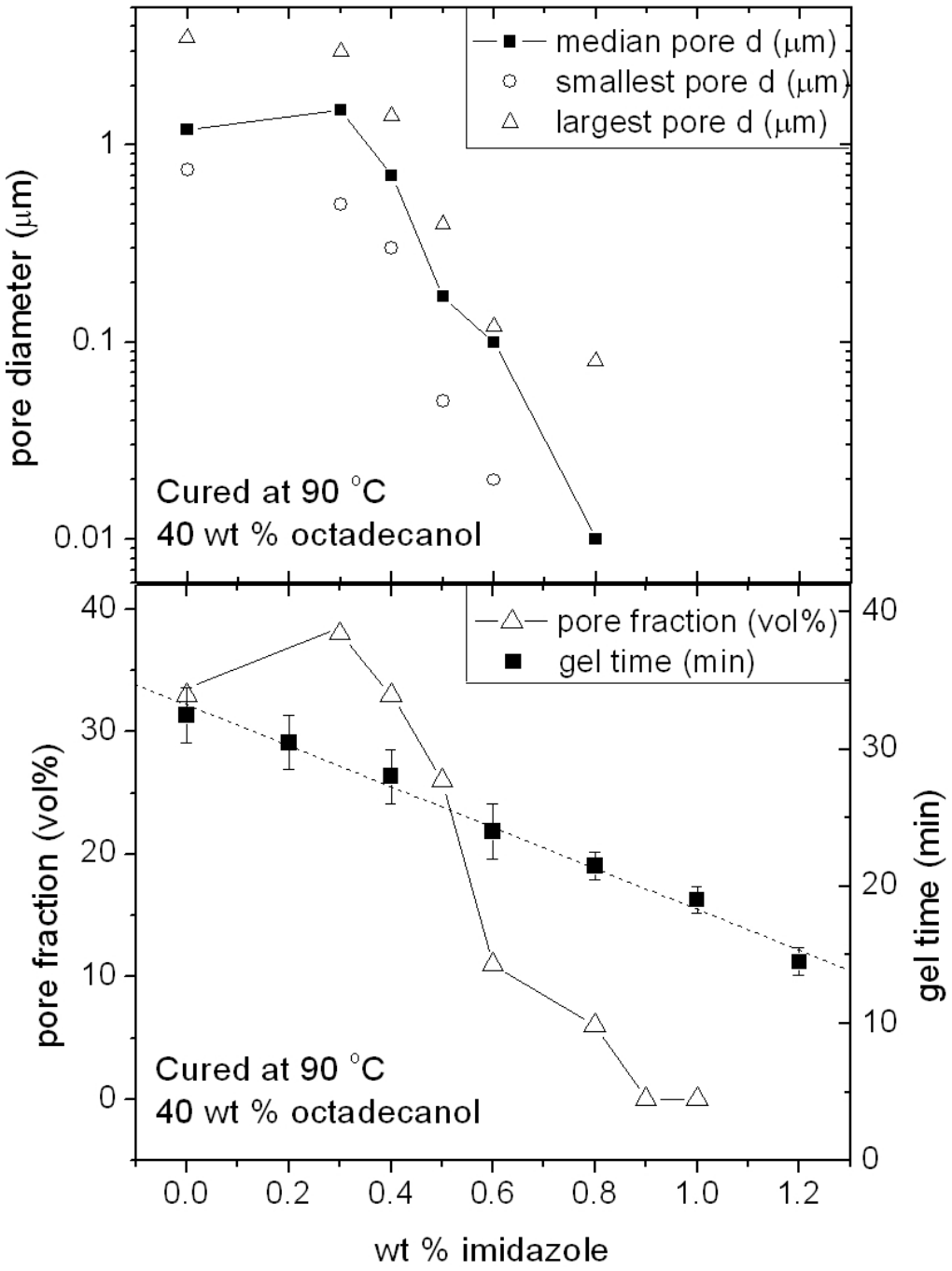

Figure 6. Pore diameter *d*, volume fraction, and gel time as a function of the amount of imidazole added relative to the amount of epoxy. All data represent a curing temperature of 90 °C and 40 wt% imidazole. The dashed line is the best linear fit to the gel times. If not shown, estimated errors are ±10 %.

Therefore, an interesting question arises when considering the decrease in pore volume fraction with increasing cure rate: after high temperature vacuum treatment, is the octadecanol that was

frozen into the matrix during cure sufficiently free to diffuse out? Vacuum treatment of thin samples containing 1 wt% imidazole and 40 wt% octadecanol at 125 ^{o}C for 48 h removed 80 % of the octadecanol, indicating that much of the excess octadecanol is not tightly bound in the cured epoxy. The minor fraction that is not removed must form strong physical bonds with the matrix and avoid evaporation. Significant concurrent cracking of the matrix occurred with octadecanol removal in the samples with no visible pores, representing unsupported shrinkage: removal of the excess
octadecanol must lead to collapse of the surrounding epoxy chains, since the temperature is significantly above the epoxy T_g. There is a slight but not major decrease in the T_g in these non-phase separated epoxies, due to an increase in free volume and dangling chain ends following octadecanol removal.

As mentioned in the introduction, CIPS can lead to either spinodal decomposition (SD) or nucleation and growth (NG) depending on several factors. In fact, in many of the previous CIPS studies, such as those by Gan et al. [31], Girard-Reydet et al. [27], Inoue et al. [21,22], and Remiro et al. [32], SD is seen at early stages of growth, and often continues to be present, leading to co-continuous morphology even in late stages of growth. In the images obtained here, SD does not manifest at any point (as far as we could observe, there was no intermediate morphology in the transition from nano-sized pores to no pores). This occurs because of the small driving force for phase separation between octadecanol and the reacting epoxy oligomers. The former is confirmed by the high fraction of octadecanol that remains in the continuous matrix even after slow cure (10-25 % of the original amount of octadecanol). The relatively large size of the alcohol, while having a negative influence on inter-diffusion rates, is shown to be a minor factor by studies that have shown high-molecular weight polymers to have the capability to phase separate into a co-continuous morphology [32,27,22].

Similar cases to the present, where NG is the only visible morphology throughout the curing process, were found by Okada et al. [33], Kiefer et al. [26,34], Siddhamalli et al. [35], and Inoue [22]. Typically, NG is found in systems with low-molecular weight components as the phase separating part, such as cyclohexane by Kiefer et al. [26] or dimethylheptanone by Plummer et al. [34]. The formation of a co-continuous network in the present work should be possible, based on theoretical considerations and prior experimental work, by increasing the reaction rate while simultaneously decreasing miscibility. The former can be achieved by increasing cure temperature or by using a more active catalyst (the influence of imidazole on reaction rate reaches a plateau near 2 wt%). The latter can be addressed by modifying the chemical structure of the small molecule so that the χ parameter of mixing increases. Preliminary experiments using alcohols of lower molecular weight (e.g., octanol and dodecanol) has led to increased miscibility, moving in the opposite direction of the SD regime. Oligomers or polymers of higher molecular weight may therefore be needed to achieve a co-continuous structure.

1.4. Summary

This paper has demonstrated a method to provide precise control of porosity over several orders of magnitude, from the micron to the nanometer scale. The sacrificial phase, octadecanol, is removed by vacuum-assisted evaporation once the epoxy components have reacted to form a

solid, porous matrix. The pore diameter is controlled through variations in cure temperature and addition of the catalyst methylimidazole.

As cure temperature decreases, pore diameter increases, likely due to an increase in the cure time (although it is difficult to rule out the additional impact of cure temperature on phase separation thermodynamics). The longer the cure time, the more time there is for the chemical components to fully diffuse into separate phases. The addition of the catalyst has a similar impact: a decrease in the cure time promotes smaller pores by quenching the phase separation in early stages. The catalyst methylimidazole promotes cure by opening epoxide rings and decreasing the energetic barrier to amine addition. Most of the excess (un-phase separated) octadecanol can be removed by prolonged heating under vacuum. Cure time decreases linearly with imidazole fraction. Only nucleation and growth, not spinodal decomposition, was observed as a phase separation mechanism in this system.

The method of chemically-induced phase-separation has been demonstrated by previous investigations. However, the importance of the present approach hinges on the simplicity of the chemical formulation, the ease by which other epoxide or amine chemistries may be substituted for the two reactive components, and the precise control of pore size down to the nanometer scale by the addition of a small amount of catalyst.

1.5. Acknowledgements

Thanks to Bonnie McKenzie for acquiring the SEM images.

1.6. References

[1] Rolison, D. R., Science 2003, 299, 1698.
[2] Adhikari, B.; Majumdar, S., Progress in Polymer Science 2004, 29, 699.
[3] Potyrailo, R. A., Angewandte Chemie International Edition 2006, 45, 702.
[4] Orellana, G.; Moreno-Bondi, M. C. (eds.), Frontiers in Chemical Sensors, Springer-Verlag, New York 2005.
[5] Xu, K., Chemical Reviews 2004, 104, 4303.
[6] Whittingham, M. S., MRS Bulletin 2008, 33, 411.
[7] Long, J. W.; Dunn, B.; Rolison, D. R.; White, H. S., Chem. Rev. 2004, 104, 4463.
[8] Zuttel, A.; Orimo, S., Mrs Bulletin 2002, 27, 705.
[9] Powell, G. L., Journal of Alloys and Compounds 2007, 446-447, 402.
[10] Freed, L. E.; Vunjaknovakovic, G.; Biron, R. J.; Eagles, D. B.; Lesnoy, D. C.; Barlow, S. K.; Langer, R., Bio-Technology 1994, 12, 689.
[11] Levesque, S. G.; Lim, R. M.; Shoichet, M. S., Biomaterials 2005, 26, 7436.
[12] Jain, A.; Rogojevic, S.; Ponoth, S.; Agarwal, N.; Matthew, I.; Gill, W. N.; Persans, P.; Tomozawa, M.; Plawsky, J. L.; Simonyi, E., Thin Solid Films 2001, 398-399, 513.
[13] Aubert, J. H.; Sylwester, A. P., Materials Technology 1994, 9, 4.
[14] de Groot, J. H.; Nijenhuis, A. J.; Bruin, P.; Pennings, A. J.; Veth, R. P. H.; Klompmaker, J.; Jansen, H. W. B., Colloid and Polymer Science 1990, 268, 1073.
[15] Jiang, P.; Hwang, K. S.; Mittleman, D. M.; Bertone, J. F.; Colvin, V. L., J. Am. Chem. Soc. 1999, 121, 11630.

[16] Li, S.; Garreau, H.; Vert, M.; Petrova, T.; Manolova, N.; Rashkov, I., Journal of Applied Polymer Science 1998, 68, 989.
[17] Lagasse, R. R.; Schroeder, J. L. 1994, in Materials Research Society Symposium Proceedings: Advances in Porous Materials, eds. S. Komarneni, D. M. Smith, J. S. Beck, vol. 371, pp. 431-436, Boston, Materials Research Society.
[18] Liu, J.; Gan, L. M.; Chew, C. H.; Teo, W. K.; Gan, L. H., Langmuir 1997, 13, 6421.
[19] Candau, F.; Pabon, M.; Anquetil, J.-Y., Colloids and Surfaces A: Physicochemical and Engineering Aspects 1999, 153, 47.
[20] Yong, C. P.; Gan, L. M. 2005, in Polymer Particles, pp. 257{298.
[21] Kim, B. S.; Chiba, T.; Inoue, T., Polymer 1993, 34, 2809.
[22] Inoue, T., Progress in Polymer Science 1995, 20, 119.
[23] Williams, R. J. J.; Rozenberg, B. A.; Pascault, J. P., Polymer Analysis - Polymer Physics 1997, 128, 95.
[24] Whinnery, L. L.; Even, W. R.; Beach, J. V.; Loy, D. A., Journal of Polymer Science Part A: Polymer Chemistry 1996, 34, 1623.
[25] Bates, F. S., Science 1991, 251, 898.
[26] Kiefer, J.; Hilborn, J. G.; Manson, J. A. E.; Leterrier, Y.; Hedrick, J. L., Macromolecules 1996, 29, 4158.
[27] Girard-Reydet, E.; Sautereau, H.; Pascault, J. P.; Keates, P.; Navard, P.; Thollet, G.; Vigier, G., Polymer 1998, 39, 2269.
[28] Baddeley, A.; Jensen, E. B. V. 2005, in Stereology for Statisticians, pp. 2.1{2.46, Chapman and Hall/CRC, New York.
[29] Dearlove, T. J., Journal of Applied Polymer Science 1970, 14, 1615.
[30] Rocks, J.; Rintoul, L.; Vohwinkel, F.; George, G., Polymer 2004, 45, 6799.
[31] Gan, W.; Yu, Y.; Wang, M.; Tao, Q.; Li, S., Macromolecular Rapid Communications 2003, 24, 952.
[32] Remiro, P. M.; Marieta, C.; Riccardi, C. C.; Mondragon, I., Polymer 2001, 42, 09909.
[33] Okada, M.; Inoue, G.; Ikegami, T.; Kimura, K.; Furukawa, H., Polymer 2004, 45, 4315.
[34] Plummer, C. J. G.; Kiefer, J., Colloid and Polymer Science 2000, 278, 736.
[35] Siddhamalli, S. K.; Kyu, T., Journal of Applied Polymer Science 2000, 77, 1257.

2. THE DEVELOPMENT OF A COMBINATORIAL/HIGH-THROUGHPUT WORKFLOW FOR THE STUDY OF POROUS POLYMER NETWORKS

2.1. Introduction

Porous polymer materials are of interest for a wide variety of applications such as tissue scaffolds,[1] controlled release,[2] chromatography,[3] low-k dielectrics,[4] separation membranes,[5] piezoelectric materials,[6] chemical sensors,[7,8] hydrogen storage materials,[9,10] and battery electrodes.[11] Several general methods for creating porous polymers have been described. These methods include conventional foaming techniques involving a non-reactive gas,[12] emulsion-templating,[13,14] thermally-induced phase separation,[15] chemically-induced phase separation,[16] selective degradation of block copolymers,[17] and molecular imprinting.[18] Relative to the other methods for producing porous polymer materials, chemically-induced phase separation (CIPS) probably provides the greatest versatility with respect to the range of materials that can be generated. In addition, the process to produce porous materials using CIPS is relatively straightforward and a large number of readily available starting materials can be utilized.

The process for producing porous polymer materials using CIPS involves crosslinking of a homogeneous blend comprised of reactive precursors and a non-reactive component referred to as a poragen.[16,19] Due to the increase in the free energy of mixing that occurs as reaction takes place between the reactive precursors, the poragen phase separates from the mixture during the process of crosslinking. Porosity is generated by removal of the poragen from the crosslinked material using an extraction or evaporation process. The pore size, pore shape, and pore size distribution obtained with this process is a result of the complex interaction between the thermodynamics of mixing, kinetics of crosslinking, and kinetics of phase separation.

The well-known Flory-Huggins[20] equation (I) that describes the free energy of mixing (ΔG_{mix}) for a blend of a polymer and solvent can be used as a basis to understand the thermodynamics of CIPS.

$$\Delta G_{mix}=RT(n_{pol}\ln ø_{pol}+ n_{sol}\ln ø_{sol}+\chi ø_{pol} n_{sol}) \qquad \text{(I)}$$

For this equation, R is the gas constant, T is temperature, n_{pol} is the number of polymer molecules in moles, n_{sol} is the number of solvent molecules in moles, $ø_{pol}$ is the volume fraction of polymer, $ø_{sol}$ is the volume fraction of solvent, and χ is the interaction parameter which accounts for intermolecular interactions between polymer and solvent molecules. χ is not a constant; it depends on temperature, composition, and pressure. Huggins[21] experimentally showed that χ varies linearly with the inverse of temperature:

$$\chi = a + b/T \qquad \text{(II)}$$

Based on χ, two basic types of phase behavior are observed. If χ is positive and increases linearly with temperature, an upper critical solution temperature (UCST) is observed. In contrast, if χ is negative and decreases linearly with temperature, a lower critical solution temperature (LCST) is observed. Figure 7 displays a representative phase diagram showing UCST behavior as well as a phase diagram showing LCST behavior. The phase diagrams

exhibit three phases, namely, a stable phase, metastable phase, and a region in which spinodal decomposition occurs. If the temperature of a stable polymer solution is changed such that the region of spinodal decomposition is entered, phase separation occurs by a mechanism which proceeds in stages, as illustrated schematically in Figure 8. Initially, a co-continuous morphology is developed which proceeds to the formation of a dispersed phase morphology. In contrast, entering the metastable region results in phase separation by a nucleation and growth mechanism in which a dispersed phase morphology consisting of spherical domains is produced.

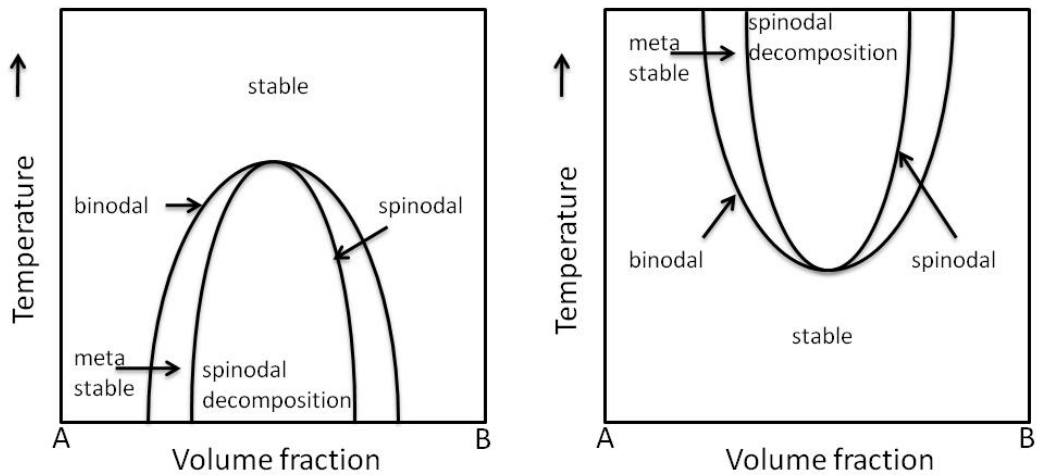

Figure 7. Representative phase diagrams showing UCST behavior (left) and LCST behavior (right).

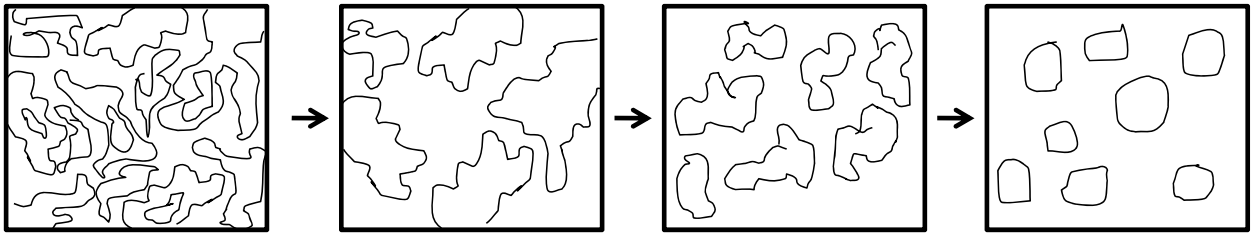

Figure 8. A schematic illustration describing morphology development associated with spinodal decomposition.

For CIPS, a stable solution is transformed into a phase separated material without a change in temperature. Phase separation in CIPS is the result of the decrease in entropy created by the increase in polymer molecular weight that occurs as a result of crosslinking reactions. Kiefer and coworkers[16] modified the Flory-Huggins equation so that it was applicable to reactive solutions. The modification took into account the change in the number of polymer molecules with functional group conversion and allowed for the construction of phase diagrams based on conversion at a constant temperature.

While thermodynamic models based on first principles are useful for identifying systems that will undergo CIPS, they do not allow for an accurate prediction of morphology because the morphology produced with CIPS depends strongly on molecular mobility which changes dramatically as crosslinking proceeds. For example, pore size for materials that undergo phase separation by a nucleation and growth mechanism will be a result of the competition that exists between the reduction in free energy achieved by the nucleation and growth of pores and the

ability of solvent molecules to diffuse through the polymer network that is increasing in viscosity as crosslinking proceeds. Due to the complexity of pore formation associated with CIPS, extensive structure-process-property relationships are needed to understand the influence of these variables on material properties.

The application of high-throughput/combinatorial methods for the generation structure-process-property relationships for polymer materials has been shown to be very powerful.[22-24] The ability to generate and characterize relatively large numbers of materials within a relatively short period of time enables the multivariable experiments required to identify complex interactions between variables. This document describes efforts to construct a high-throughput/combinatorial workflow for the generation of extensive structure-process-property relationships for porous polymer materials produced with the process of CIPS. In addition, results obtained for a relatively large experiment involving porous epoxy networks is described.

2.2. Experimental

2.2.1. Materials

Table I describes the materials used for the experiment, and Table II describes each of the blends prepared.

Table 1. A description of the starting materials used for the study.

Material ID	Description	Trade Name	Manufacturer
Ep	Bisphenol –A- diglycidylether	Epon™ Resin 825	Hexion
Lxl	Amino-terminated polypropylene glycol with molecular weight 230 g/mol	Jeffamine® D-230	Huntsman
Mxl	Amino-terminated polypropylene glycol with molecular weight 430 g/mol	Jeffamine® D-400	Huntsman
Hxl	Amino-terminated polypropylene glycol with molecular weight 2000 g/mol	Jeffamine® D-2000	Huntsman
MCHA	4,4'-methylenebis(cyclohexylamine)	----	Aldrich
De	Decane	----	Aldrich
Dol	n-Decanol	----	Aldrich
PMA	Propylene glycol methyl ether acetate	----	Aldrich
EEP	Ethyl-3-ethoxy propionate	----	Aldrich
MAK	2-Heptanone	----	Aldrich
DBK	2,6-Dimethyl-4-heptanone	----	Aldrich

Table 2. Composition of the each of the blends prepared. All weights are in grams.

Sample ID	Wt. Ep	Crosslinker	Wt. Crosslinker	Poragen	Wt. Poragen
Lxl-10De	7.00	Lxl	2.33	De	0.70
Lxl-10Dol	7.00	Lxl	2.33	Dol	0.80
Lxl-10PMA	7.00	Lxl	2.33	PMA	0.88
Lxl-10EEP	7.00	Lxl	2.33	EEP	0.91
Lxl-10MAK	7.00	Lxl	2.33	MAK	0.79
Lxl-10DBK	7.00	Lxl	2.33	DBK	0.76

Lxl-25De	7.00	Lxl	2.33	De	2.10
Lxl-25Dol	7.00	Lxl	2.33	Dol	2.39
Lxl-25PMA	7.00	Lxl	2.33	PMA	2.64
Lxl-25EEP	7.00	Lxl	2.33	EEP	2.73
Lxl-25MAK	7.00	Lxl	2.33	MAK	2.36
Lxl-25DBK	7.00	Lxl	2.33	DBK	2.32
Lxl-40De	7.00	Lxl	2.33	De	4.20
Lxl-40Dol	7.00	Lxl	2.33	Dol	4.77
Lxl-40PMA	7.00	Lxl	2.33	PMA	5.28
Lxl-40EEP	7.00	Lxl	2.33	EEP	5.47
Lxl-40MAK	7.00	Lxl	2.33	MAK	4.72
Lxl-40DBK	7.00	Lxl	2.33	DBK	4.65
Mxl-10De	7.00	Mxl	4.47	De	0.89
Mxl-10Dol	7.00	Mxl	4.47	Dol	1.01
Mxl-10PMA	7.00	Mxl	4.47	PMA	1.12
Mxl-10EEP	7.00	Mxl	4.47	EEP	1.16
Mxl-10MAK	7.00	Mxl	4.47	MAK	1.00
Mxl-10DBK	7.00	Mxl	4.47	DBK	0.98
Mxl-25De	7.00	Mxl	4.47	De	2.66
Mxl-25Dol	7.00	Mxl	4.47	Dol	3.03
Mxl-25PMA	7.00	Mxl	4.47	PMA	3.35
Mxl-25EEP	7.00	Mxl	4.47	EEP	3.47
Mxl-25MAK	7.00	Mxl	4.47	MAK	2.99
Mxl-25DBK	7.00	Mxl	4.47	DBK	2.95
Mxl-40De	7.00	Mxl	4.47	De	5.33
Mxl-40Dol	7.00	Mxl	4.47	Dol	6.05
Mxl-40PMA	7.00	Mxl	4.47	PMA	6.70
Mxl-40EEP	7.00	Mxl	4.47	EEP	6.94
Mxl-40MAK	7.00	Mxl	4.47	MAK	5.99
Mxl-40DBK	7.00	Mxl	4.47	DBK	5.90
Hxl-10De	3.50	Hx1	9.99	De	1.15
Hxl-10Dol	3.50	Hx1	9.99	Dol	1.30
Hxl-10PMA	3.50	Hx1	9.99	PMA	1.44
Hxl-10EEP	3.50	Hx1	9.99	EEP	1.49
Hxl-10MAK	3.50	Hx1	9.99	MAK	1.29
Hxl-10DBK	3.50	Hx1	9.99	DBK	1.27
Hxl-25De	3.50	Hx1	9.99	De	3.44
Hxl-25Dol	3.50	Hx1	9.99	Dol	3.91
Hxl-25PMA	3.50	Hx1	9.99	PMA	4.33
Hxl-25EEP	3.50	Hx1	9.99	EEP	4.48
Hxl-25MAK	3.50	Hx1	9.99	MAK	3.87
Hxl-25DBK	3.50	Hx1	9.99	DBK	3.81
Hxl-40De	3.50	Hx1	9.99	De	6.88
Hxl-40Dol	3.50	Hx1	9.99	Dol	7.82
Hxl-40PMA	3.50	Hx1	9.99	PMA	8.66

Hxl-40EEP	3.50	Hx1	9.99	EEP	8.96
Hxl-40MAK	3.50	Hx1	9.99	MAK	7.73
Hxl-40DBK	3.50	Hx1	9.99	DBK	7.62
MCHA-10De	7.00	MCHA	2.04	De	0.66
MCHA-10Dol	7.00	MCHA	2.04	Dol	0.75
MCHA-10PMA	7.00	MCHA	2.04	PMA	0.84
MCHA-10EEP	7.00	MCHA	2.04	EEP	0.86
MCHA-10MAK	7.00	MCHA	2.04	MAK	0.75
MCHA-10DBK	7.00	MCHA	2.04	DBK	0.74
MCHA-25De	7.00	MCHA	2.04	De	1.99
MCHA-25Dol	7.00	MCHA	2.04	Dol	2.26
MCHA-25PMA	7.00	MCHA	2.04	PMA	2.51
MCHA-25EEP	7.00	MCHA	2.04	EEP	2.59
MCHA-25MAK	7.00	MCHA	2.04	MAK	2.24
MCHA-25DBK	7.00	MCHA	2.04	DBK	2.21
MCHA-40De	7.00	MCHA	2.04	De	3.98
MCHA-40Dol	7.00	MCHA	2.04	Dol	4.52
MCHA-40PMA	7.00	MCHA	2.04	PMA	5.01
MCHA-40EEP	7.00	MCHA	2.04	EEP	5.19
MCHA-40MAK	7.00	MCHA	2.04	MAK	4.48
MCHA-40DBK	7.00	MCHA	2.04	DBK	4.41

2.2.2. Instrumentation

SEM images were taken with the JEOL JSM-6300 scanning electron microscope available at NDSU or with a FEG-SEM JEOL 6700 that was available within the Characterization Facility at the University of Minnesota.

2.3. Results and Discussion

2.3.1. Description of the High-throughput/Combinatorial Workflow Developed

Figure 9 provides a schematic illustration of the high-throughput workflow that was developed. With this workflow, experimental designs are created using Design-Expert® software and the designs transferred into Symyx Library Studio® which is used by Epoch® to control the formulation robot. Blends of the polymer network-forming precursors and poragen are prepared robotically using a Symyx viscous liquid handling formulation system and in-house modification that allows for the use of disposable vessels. 24 liquid blends are prepared at one time. Figure 10 displays an image of the robotic system used for preparing liquid blends.

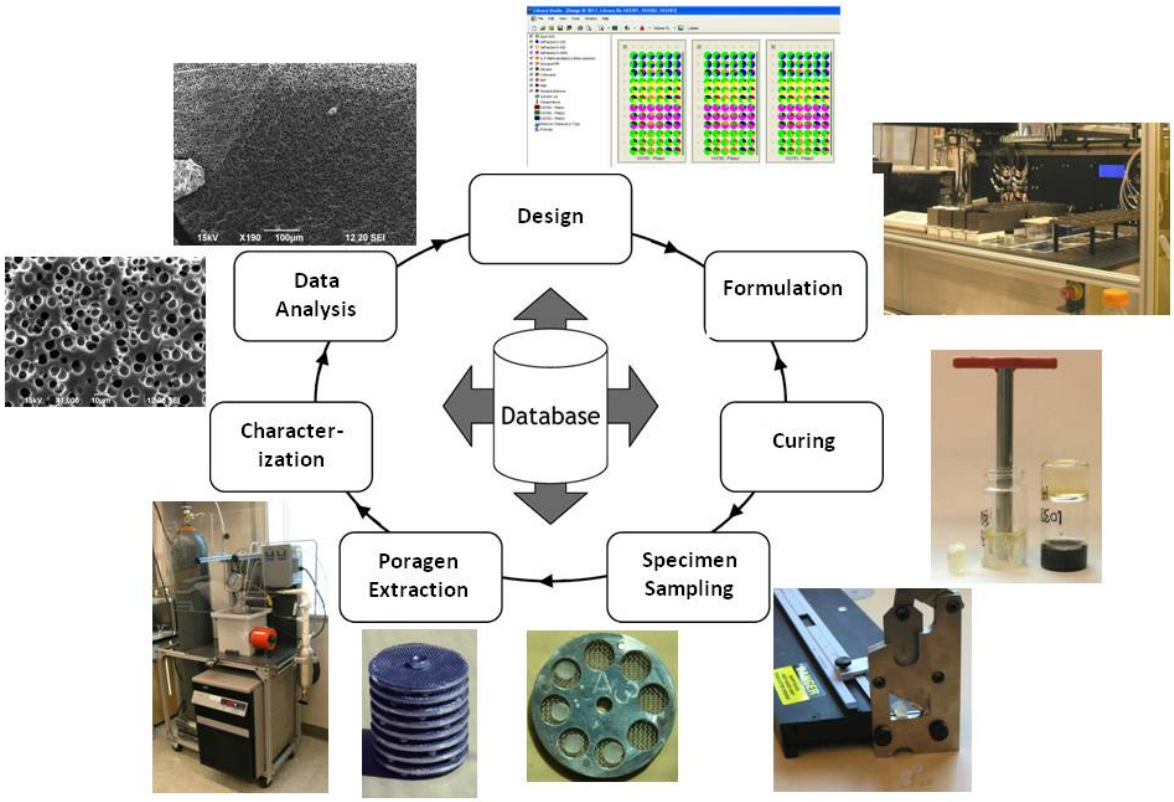

Figure 9. A schematic illustration of the high-throughput workflow that was developed.

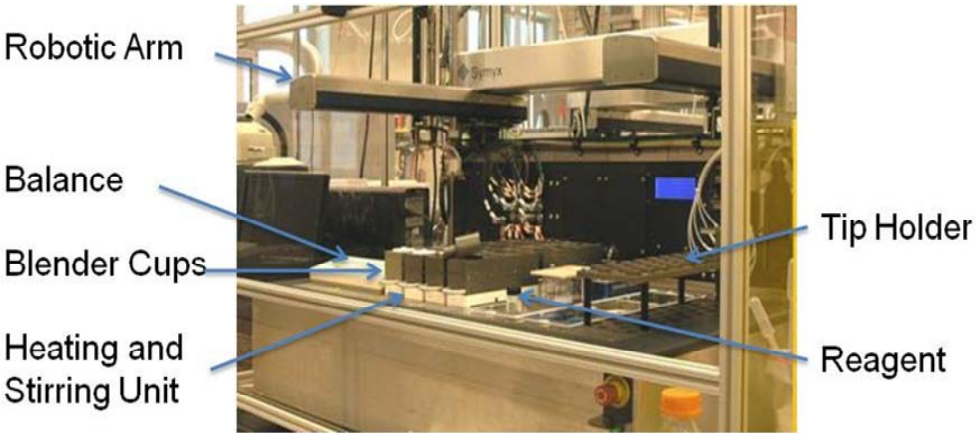

Figure 10. An image of the robotic system used for preparing liquid blends.

Once the liquid blends are prepared, they are transferred to 20 mL glass vials for the cure step. Each glass vial is filled with approximately 10 mLs of liquid blend and the vial capped. The capped vials are then placed in a forced air oven to cure. Once cured, the samples are allowed to cool to room temperature before extracting a cylinderical specimen from each sample using the boring device shown in Figure 11. From the cylindrical specimen, discs approximately 1.0 mm in diameter and 2.0 mm thick are prepared by slicing with a lever-action slicer (Figure 11). The weight of each disc is measured with the assistance of a Bhodan® weighing robot.

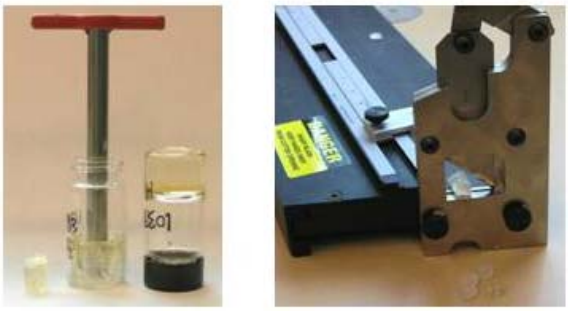

Figure 11. An image of the boring device used to extract cylindrical specimens of cured material (left) and the device used for preparing sample discs from the cylindrical specimen (right).

Once the sample discs are weighed, the poragen is extracted using super critical CO_2 and the device shown in Figure 12. This device consists of a Parr™ pressure vessel fitted with a 64 position sample holder. Liquid CO_2 is fed into the vessel in batch fashion through a dip tube in the CO_2 supply cylinder. The vessel is then heated above the critical point using a circulating water bath for stable control of the extraction temperature. To ensure effective poragen removal, the extracted sample discs are reweighed with the weighing robot and the weight loss resulting from extraction compared to the weight of poragen used to prepare the material.

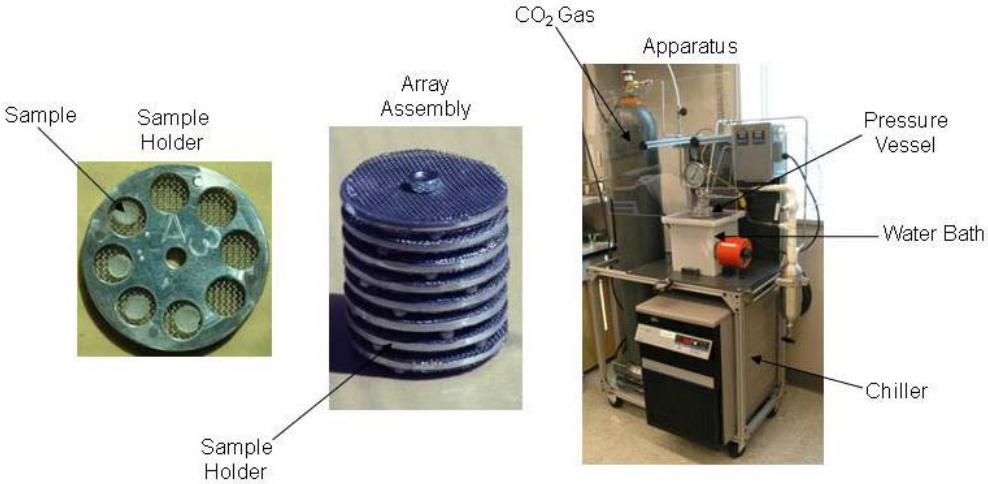

Figure 12. An image of the device used for poragen extraction of an array of 64 samples.

A few different methods such as BET (Brunauer, Emmett and Teller) surface area measurements using both nitrogen and krypton gas were investigated for characterizing the porosity of the samples, but SEM was the only method that provided adequate information on material morphology. Unfortunately, conventional SEM is not a high-throughput method and, thus, the characterization component of the high-throughput workflow was a "bottle-neck" in the process that will need to be addressed in future work (see the Conclusions/Future Work section).

2.3.2. Porous Epoxy Networks Produced Using CIPS

An experiment was designed to investigate the effects of various compositional factors as well as cure temperature on the porosity of porous epoxy networks produced using CIPS. The epoxy-functional precursor used for the study was the diglycidyl ether of bisphenol A (Ep). In order to

investigate the effect of crosslink density on material properties, a series of amino-terminated polypropylene glycol oligomers of varying molecular weight were used for crosslinking. Figure 13 provides a schematic illustrating the formation of the crosslinked network. For all samples, the molar ratio of epoxy-groups to amino-groups was kept constant at 1:2. In addition to the series of amino-terminated PEG oligomers, 4,4'-methylenebis(cyclohexylamine) (MCHA) was used as an additional crosslinker in the study.

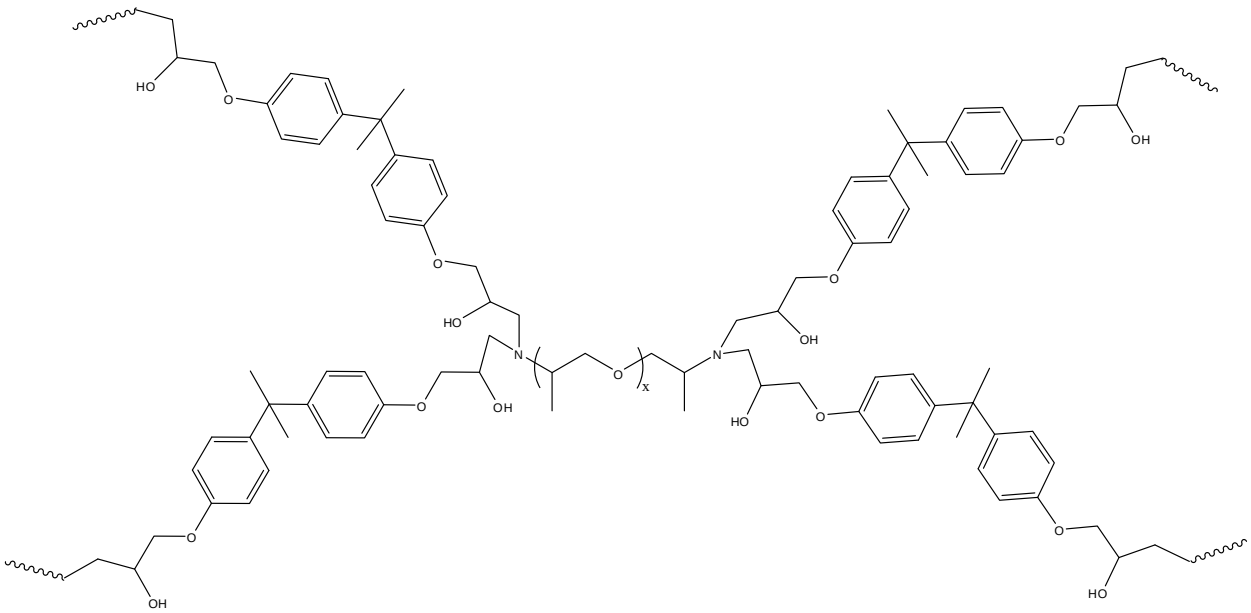

Figure 13. A schematic illustrating the formation of the crosslinked network.

A series of poragens possessing systematic variations in chemical structure were used for the experiment. As shown in Table III, the molecular size of the poragens was similar, but the characteristics of their solubility parameter varied considerably. Based on thermodynamic considerations, it was expected that the use of this series of poragens would result in a range of behavior with respect to the process of CIPS. In addition to poragen chemical composition, poragen concentration was varied at 10, 25, and 40 percent by volume.

Table 3. Solubility parameters for poragens, polymer network-forming precursors, and polymer network.

Compounds	Chemical Structure	BP (ºC)	Solubility parameter $(J/cm^3)^{½}$			
			Δ	δ_d	δ_p	δ_h
De	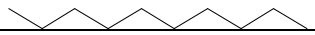	174	15.4	15.4	0.0	0.0
Dol	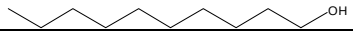	231	20.4	17.6	2.7	10.0
PMA	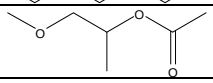	146	18.4	16.1	6.1	6.6
EEP	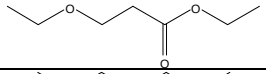	170	19.6	16.2	3.3	8.8
MAK	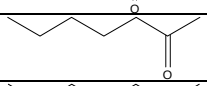	151	17.6	16.2	5.7	4.1
DBK	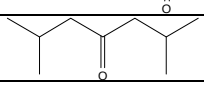	165-170	16.1	15.2	4.4	3.4

Ep	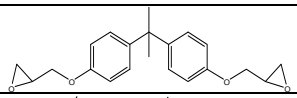	----	18.2	16.9	1.4	6.4
Lxl	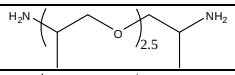	----	17.1	14.2	6.5	7.0
Mxl	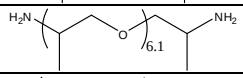	----	17.5	14.6	6.7	7.1
Hxl	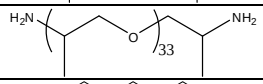	----	17.8	14.8	6.8	7.2
MCHA	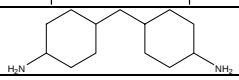	----	20.3	18.3	0.0	8.7
Ep-Lx1	Crosslinked network	----	19.9	17.1	3.7	9.5
Ep-Mx1	Crosslinked network	----	18.9	16.1	4.8	8.6
Ep-Hx1	Crosslinked network	----	18.8	15.9	6.5	7.7
EP-MCHA	Crosslinked network	----	20.4	18.9	1.4	7.5

In addition to the compositional variables described above, cure temperature was varied at 40, 80, and 120 °C. Figure 14 displays a schematic illustrating the overall experimental design. A total of 216 unique compositions were used for the study. The convention used to identify the materials prepared is as follows:

a-bc-d

where “a” is the composition of the crosslinker, “b” is the volume percent of the poragen, “c” is the composition of the poragen, and “d” is the cure temperature in degrees Celsius.

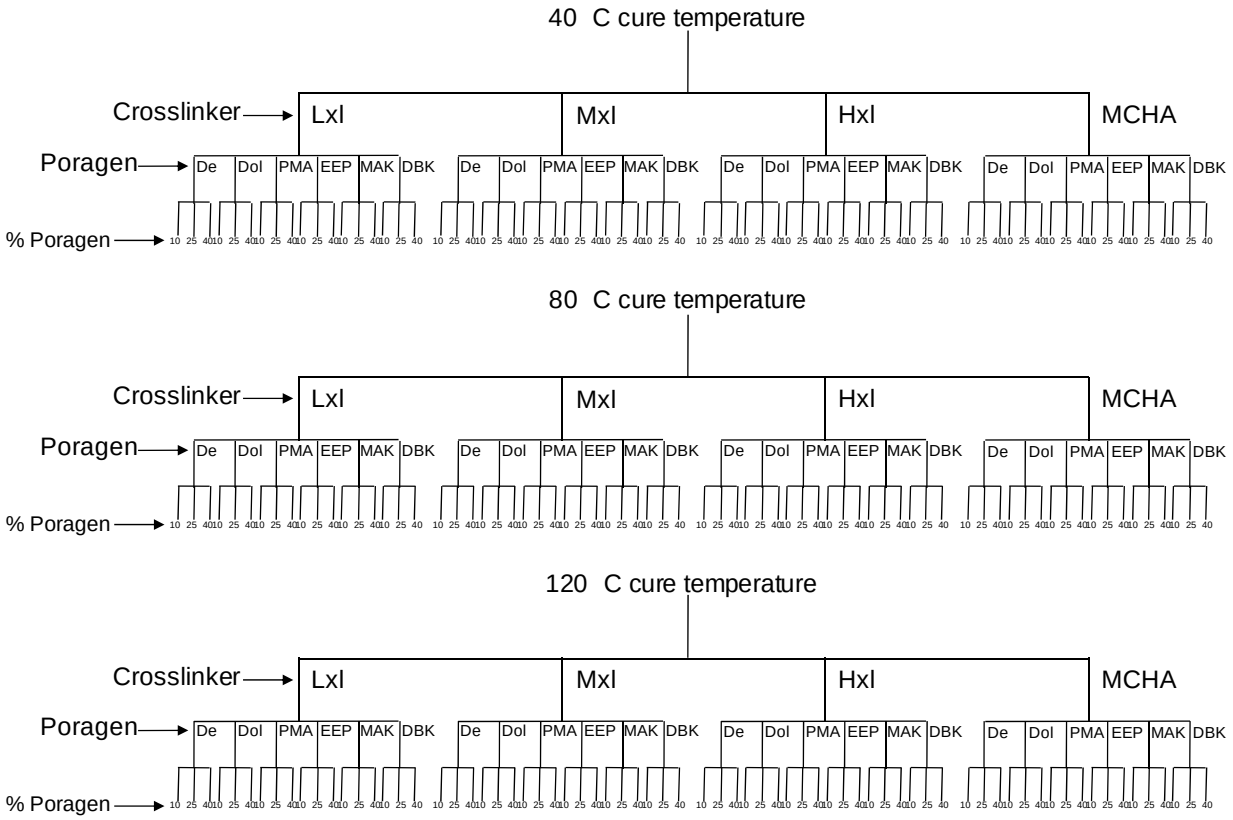

Figure 14. A schematic illustration of the experimental design used for the study.

Prior to producing the entire set of 216 materials containing poragen, samples of the thermoset matrix (no poragen) were prepared and characterized. All crosslinkers were miscible with Ep and cured materials were obtained at all three cure temperatures of interest (40, 80, and 120 °C). As shown in Figure 15, Tgs decreased exponentially with crosslinker equivalent weight (g/mole NH_2) over a wide range temperature range. No significant differences were observed between Tg and cure temperature indicating that "full" cure was obtained at all three cure temperatures. In addition, as shown in Figure 16, fractures surface were essentially featureless at the micron-scale.

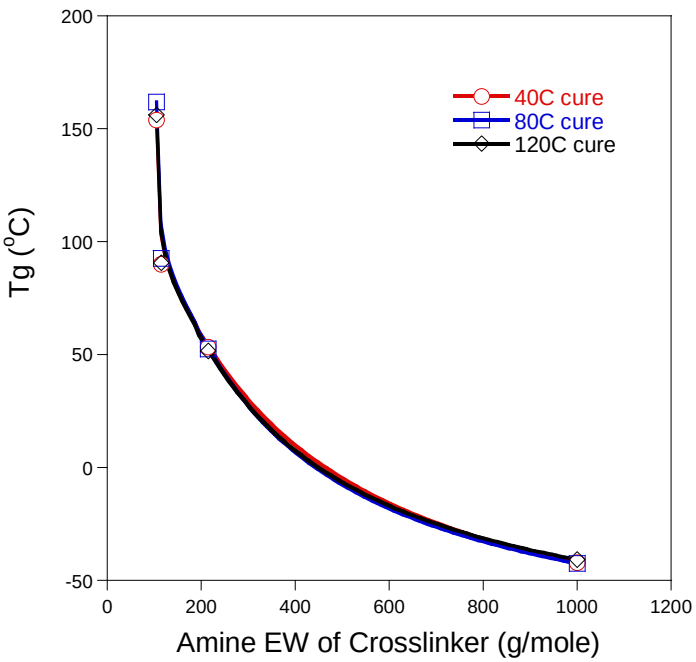

Figure 15. Tg as a function of crosslinker equivalent weight (g/mole NH_2) for the cured polymer networks (no poragen).

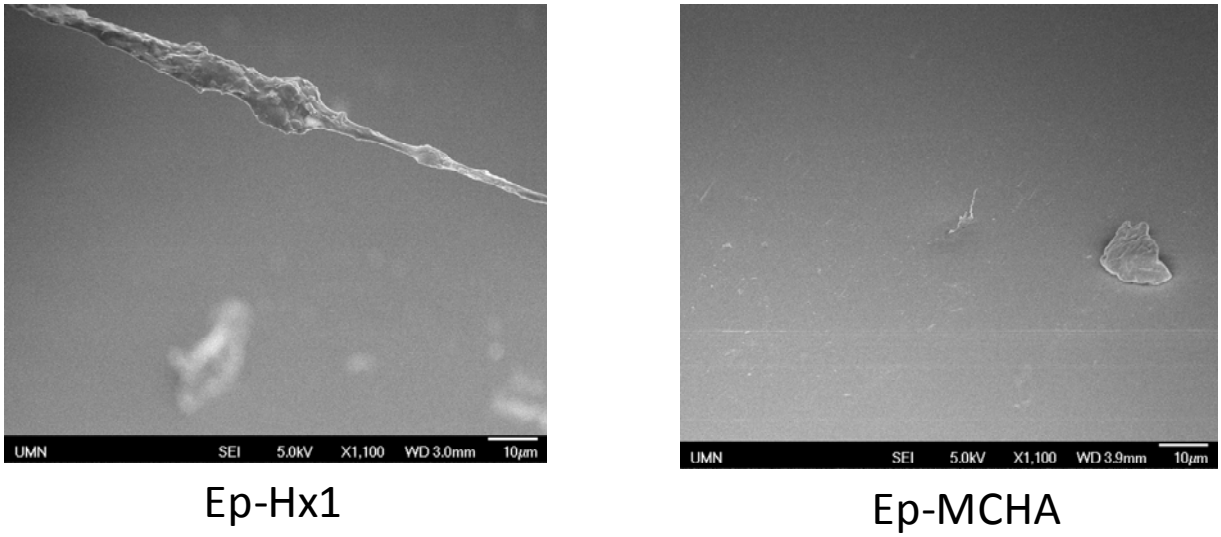

Figure 16. SEM images of fracture surfaces obtained from cured polymer networks (no poragen).

For the production of porous polymer materials using the process of CIPS, it is necessary that the uncured blend of Ep, crosslinker, and poragen be miscible prior to curing. Thus, observations of blend miscibility were made shortly after robotic preparation of the blends. As shown in Table IV, all blends based on PMA, EEP, MAK, and DBK were fully miscible at room temperature while limited miscibility was observed for blends based on De and Dol. For blends based on De, only two materials were miscible at room temperature, namely, Mxl-10De and Hxl-10De. For blends based on Dol, those containing Dol concentrations of 40 percent were immiscible while

those containing Dol concentrations of 25 and 10 percent were miscible at room temperature. To explain the variations in blend miscibility observed, the solubility parameters for Ep and the various crosslinkers were calculated using the group-contribution method.[25] As shown in Table III, the solubility parameter for Ep and the amino-terminated polypropylene glycol crosslinkers was 18.2 and 17.1-17.8, respectively. A comparison of these solubility parameters to those of the poragens showed that the greatest difference in solubility parameter was observed for De and Dol which was consistent with the miscibility results observed.

Table 4. Results of observations made at room temperature regarding blend miscibility. "+" indicates the formation of a miscible blend while "-" indicates the formation of a two-phase blend.

Matrix (crosslinker)	v% Poragen	Poragen					
		De	Dol	PMA	EEP	MAK	DBK
Lxl	10	-	+	+	+	+	+
	25	-	+	+	+	+	+
	40	-	-	+	+	+	+
Mxl	10	+	+	+	+	+	+
	25	-	+	+	+	+	+
	40	-	-	+	+	+	+
Hxl	10	+	+	+	+	+	+
	25	-	+	+	+	+	+
	40	-	-	+	+	+	+
MCHA	10	-	+	+	+	+	+
	25	-	+	+	+	+	+
	40	-	-	+	+	+	+

Due to differences in cure rate resulting from differences in reactive group concentration, the time required to cure the blends into solid materials varied substantially. For example, at the highest cure temperature (120 °C), blends based on the lowest poragen concentration and lowest molecular weight crosslinker cured to a solid material in less than 72 hours while blends cured at the lowest cure temperature (40 °C) and based on the highest poragen concentration and highest molecular weight crosslinker required approximately 21 days to cure to a solid material. Due to these variations in cure rate, observations were periodically made to ensure that all blends had sufficiently cured before removing them from the oven.

Once cured, observations were made with regard to the phase characteristics of the materials. As shown in Figure 11, three basic types of phase behavior were visually observed for the blends. The production of transparent, homogeneous blends (Figure 17a) indicated complete miscibility while the production of a stable emulsion (Figure 17b) or a two layer solution (Figure 17c) indicated immiscibility. As shown in Table V, 79 % of the materials were transparent (Figure 17a) indicating homogeneity at the macroscopic level, 16 % formed two separate layers in which the poragen separated from the cured polymer to produce a liquid layer above the cured polymer (Figure 17c), and 5 % formed opaque materials in which the poragen existed as large domains within the crosslinked polymer (Figure 17b). As expected, the occurrence of macroscopic phase separation was strongly related to the composition of the poragen. All of the materials based on

MAK or Dowanol-PM were transparent while macroscopic phase separation occurred for 72 % of the materials based on decane. Since the enthalpy of mixing is related to the difference in solubility parameter between a solvent and polymer, the number of macroscopically phase separated materials observed for a given poragen was plotted as function of the solubility parameter of the poragen. As shown in Figure 12, the plot exhibits a minimum at a solubility parameter of about 18.5. For comparison, the solubility parameter of the four different crosslinked matrices were calculated using the group contribution method.[25] As shown in Table III, the solubility parameters for the four different crosslinked networks were 20.4, 19.9, 18.9, and 18.8 for Ep-MCHA, Ep-Lxl, Ep-Mxl, and Ep-Hxl, respectively. Considering the solubility parameters calculated for the crosslinked networks, it is not surprising that the poragens possessing a solubility parameter close to 18.5 gave the lowest occurrence of micron-scale phase separation.

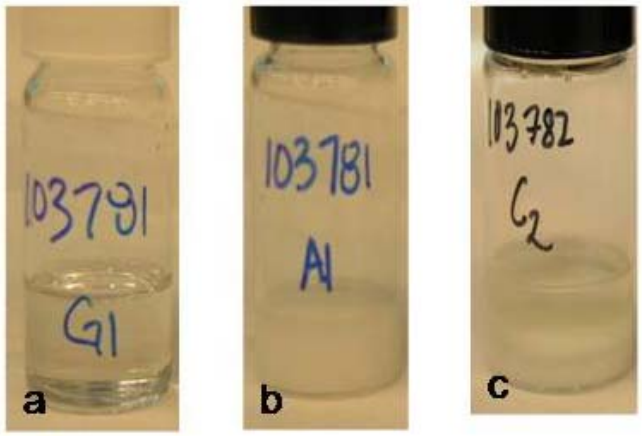

Figure 17. Images illustrating the various types of phase behavior exhibited by blends at room temperature.

In addition to the phase behavior for the cured materials, the phase behavior of the uncured blends at room temperature was plotted in Figure 18. A comparison of the phase behavior exhibited before and after curing indicated that curing did not induce macroscopic phase separation for any of the materials based on PMA (δ = 18.4) or MAK (δ = 17.6); however, curing did induce macroscopic phase separation for blends based on DBK (δ = 16.1) and EEP (δ = 19.6). Examination of the data displayed in Tables IV and V show that all of the materials that underwent macroscopic phase separation as a result of curing were based on the high level (40 %) of poragen. The data in Figure 12 also indicates that some uncured blends based on De and Dol that were immiscible at room temperature formed transparent materials when cured. This result suggests that, when heated to the curing temperature, the liquid blend transformed from a two phase material to a miscible blend prior to undergoing crosslinking and CIPS did not occur. The transformation of a two-phase liquid blend to a miscible blend upon heating is consistent with USCT behavior expected for the liquid blends.[16] A comparison of the data displayed in Tables IV and V show that this behavior was obtained for 17% of the samples based on De or Dol as the poragen. For future work, it would be useful to observe the phase behavior of the blends at the cure temperature prior to gelation. This is addressed in the "Conclusions and Future Work" section.

Table 5. Results of visual observations made regarding the phase behavior of the cured materials. "T" indicates the observation shown in Figure 11a, "O" indicates the observation shown in Figure 11b, and "2L" indicates the observation shown in Figure 11c.

Matrix (crosslinker)	% poragen	Poragen																	
		De			Dol			PMA			EEP			MAK			DBK		
		Cure (°C)			Cure (°C)			Cure (°C)			Cure (°C)			Cure (°C)			Cure (°C)		
		40	80	120	40	80	120	40	80	120	40	80	120	40	80	120	40	80	120
Lxl	10	O	O	T	T	T	T	T	T	T	T	T	T	T	T	T	T	T	T
	25	2L	2L	2L	T	T	T	T	T	T	T	T	T	T	T	T	T	T	T
	40	2L	2L	2L	2L	2L	O	T	T	T	T	T	2L	T	T	T	O	2L	2L
Mxl	10	O	T	T	T	T	T	T	T	T	T	T	T	T	T	T	T	T	T
	25	2L	2L	2L	T	T	T	T	T	T	T	T	T	T	T	T	T	T	T
	40	2L	2L	2L	2L	T	2L	T	T	T	T	T	T	T	T	T	T	T	2L
Hxl	10	T	T	T	T	T	T	T	T	T	T	T	T	T	T	T	T	T	T
	25	T	T	T	T	T	T	T	T	T	T	T	T	T	T	T	T	T	T
	40	2L	2L	2L	T	T	T	T	T	T	T	T	T	T	T	T	T	T	T
MCHA	10	O	T	2L	T	T	T	T	T	T	T	T	T	T	T	T	T	T	T
	25	2L	2L	2L	T	T	T	T	T	T	T	T	T	T	T	T	O	T	T
	40	2L	2L	2L	O	2L	2L	T	T	T	O	T	2L	T	T	T	O	O	2L

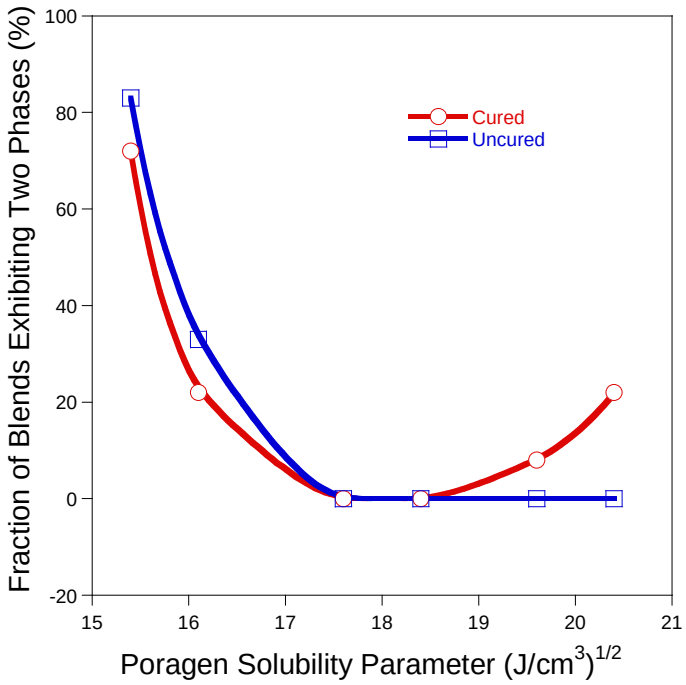

Figure 18. Phase behavior of uncured blends at room temperature and fully cured blends as a function of poragen solubility parameter.

Monolithic discs of the samples were extracted with supercritical CO_2 and the extraction process monitored by periodically weighing the discs using a robotic weighing instrument. Extraction time was adjusted based on results obtained from sample weighing to ensure full extraction of the poragen. Since SEM, the method needed to characterize sample morphology, is relatively time and resource intensive, subsets of the 216 samples were selected for extraction and porosity characterization. The initial material subset characterized consisted of 24 samples based on a single crosslinker (Hxl), all six poragens, two poragen concentrations (10 and 40 vol. %), and two temperatures (40 and 120 °C). Figure 13 displays representative SEM images of fracture surfaces for each of the 24 samples. The images displayed in Figure 13 show three basic

morphologies. For many samples, such as Hxl-10PMA-120C, Hxl-40PMA-40C, and Hxl-40EEP-40C, smooth, featureless fracture surfaces equivalent to those observed for the control samples (no poragen) were obtained. This morphology indicates that the material remained a stable, one phase material over the course of crosslinking. Samples Hxl-40Dol-120C, Hxl-40De-40C, and Hxl-40De-120C exhibit spherical pores consistent with CIPS occurring by a nucleation and growth mechanism. The final general morphology that was observed for samples such as Hxl-40PMA-120C, Hxl-40PMA-120C, and Hxl-40MAK-120C consists of a rough fracture surface in which discrete pores were not observed. This morphology may be the result of quenching phase separation at the early stage of the phase separation process by the increase in viscosity and reduction in molecular mobility associated with the process of crosslinking. In general, the results shown in Figure 19 indicate that increasing poragen concentration and increasing cure temperature increase the tendency for the formation of a two-phase morphology; however, micron-scale pores were only observed for materials based on the two poragens which showed the lowest miscibility with the reactive precursors, namely, De and Dol. Assuming USCT behavior for the blend of the poragen and uncured polymer (polymer that has not yet gelled), the observation that increasing temperature promoted phase separation indicates that the increase in polymer molecular weight resulting from crosslinking reactions has a bigger effect on thermodynamics of mixing than the temperature effect.

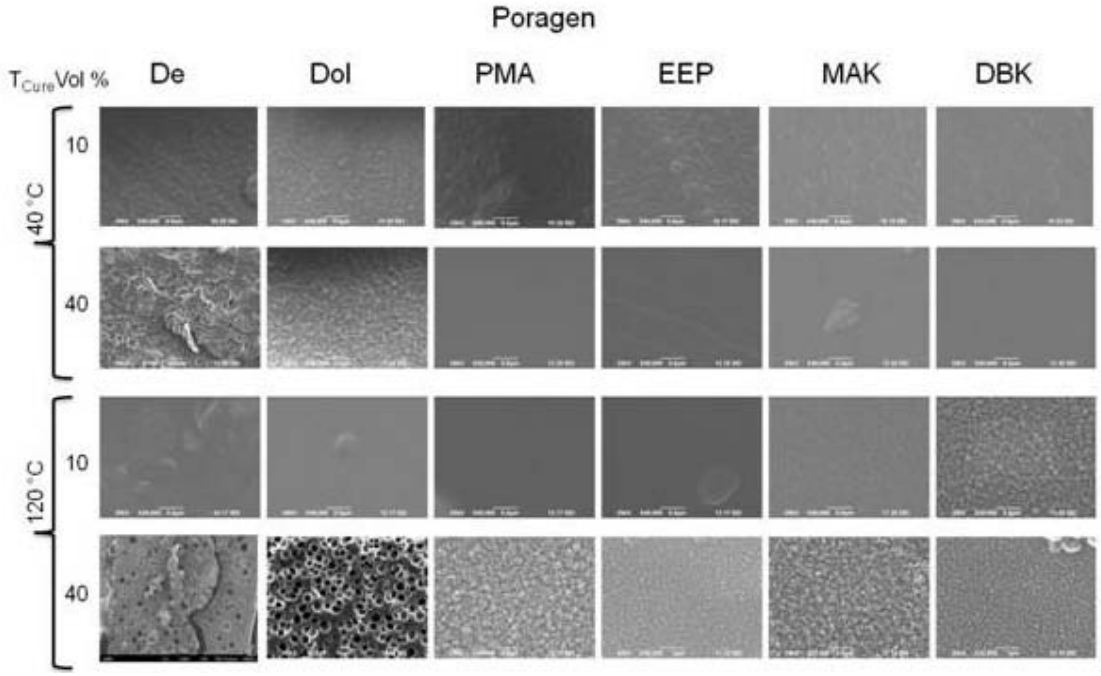

Figure 19. Representative images of fracture surfaces for 24 different samples.

The SEM used to generate the images shown in Figure 13 was not capable of characterizing morphology at the nanoscale. As a result, a small subset of materials were taken to the University of Minnesota and characterized using a Field-Emission SEM. Figures 14 and 15 display images of materials that illustrate both micron-scale features and nano-scale features. At the nanoscale, no pores were identified, but channel or crack-like features were observed for the materials based on Hxl as the crosslinker (Figure 20). For analogous materials based on MCHA as the crosslinker (Figure 21), these crack-like features were not observed indicating an effect of polymer network composition on nanoscale morphology.

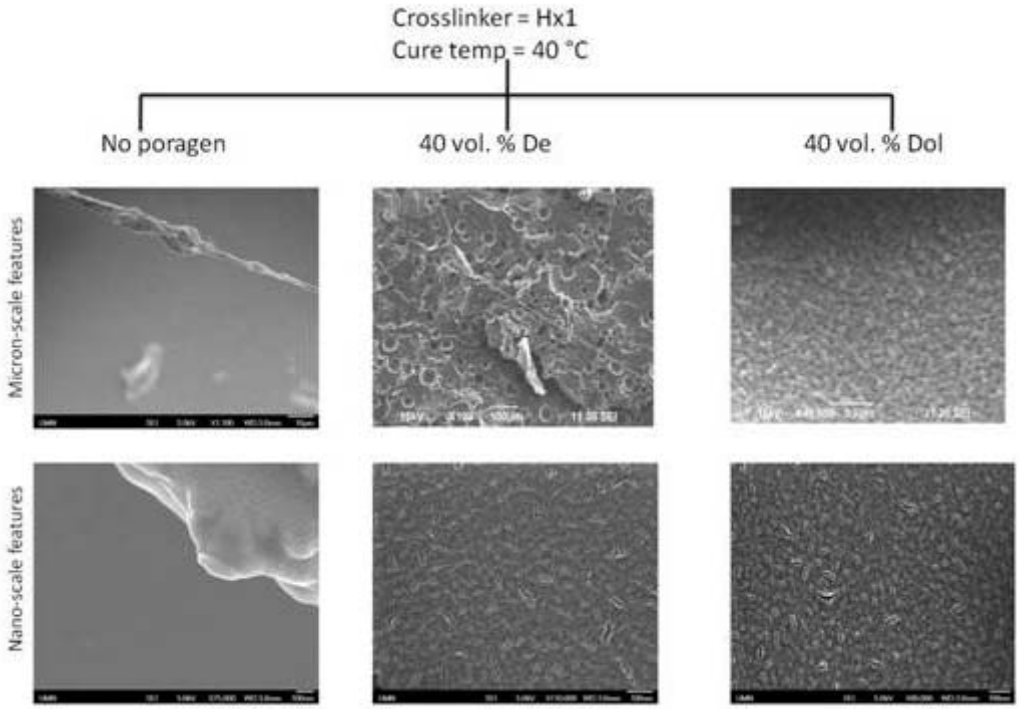

Figure 20. SEM images of fracture surfaces of materials based on Hxl as the crosslinker and cured at 40 °C.

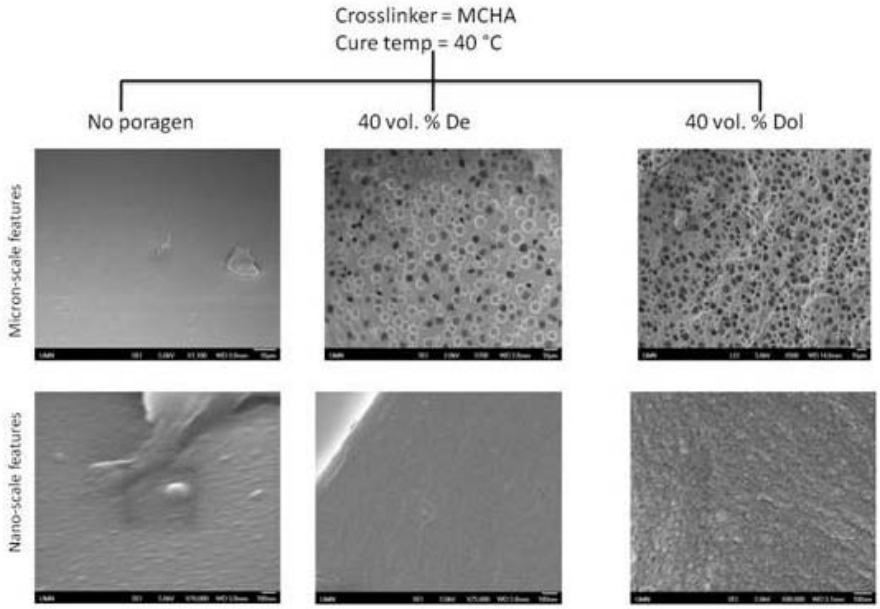

Figure 21. SEM images of fracture surfaces of materials based on MCHA as the crosslinker and cured at 40 °C.

2.4. Conclusions and Future Work

The primary objective of the project was to apply high-throughput/combinatorial methods to the study of porous polymer materials produced by CIPS. With the exception of the development of a high-throughput method of characterizing material porosity and morphology, this objective was accomplished. Samples were readily prepared using existing robotic material formulation equipment and a custom-built poragen extraction apparatus designed to simultaneously extract 64 samples. SEM is perhaps the best method for obtaining detailed morphological information, but traditional SEM techniques are low-throughput. For future work, the utility of a commercially-available high-throughput SEM from FEI Company could be investigated.[26]

Using the high-throughput approach, a relatively large number of materials were prepared in a relatively short period of time. The results obtained allowed for the identification of the appropriate poragens and process conditions required to obtain porosity. In general, the use of the two poragens that exhibited limited miscibility with the polymer network precursors (De and Dol) and relatively high levels of poragen produced micron-scale porosity. Due to throughput and cost limitations associated with SEM, only a subset of materials was characterized with regard to material morphology. For detailed structure-process-property relationships, characterization of all or a larger portion of the materials produced is needed.

To further enhance throughput and obtain additional data related to phase behavior, a new concept for generating cured materials is being developed that should enable changes in macroscopic phase behavior to be directly observed as a function of material composition, temperature, and cure time. The method involves the construction of a gradient array in which a temperature gradient will be generated by heating one end of a copper plate and cooling the other end. An array of o-rings will be mounted to the top of the gradient plate to create individual wells for samples. The o-rings will be sealed with a glass cover plate to prevent solvent loss due to evaporation. Figure 22 provides a detailed drawing of the assembly.

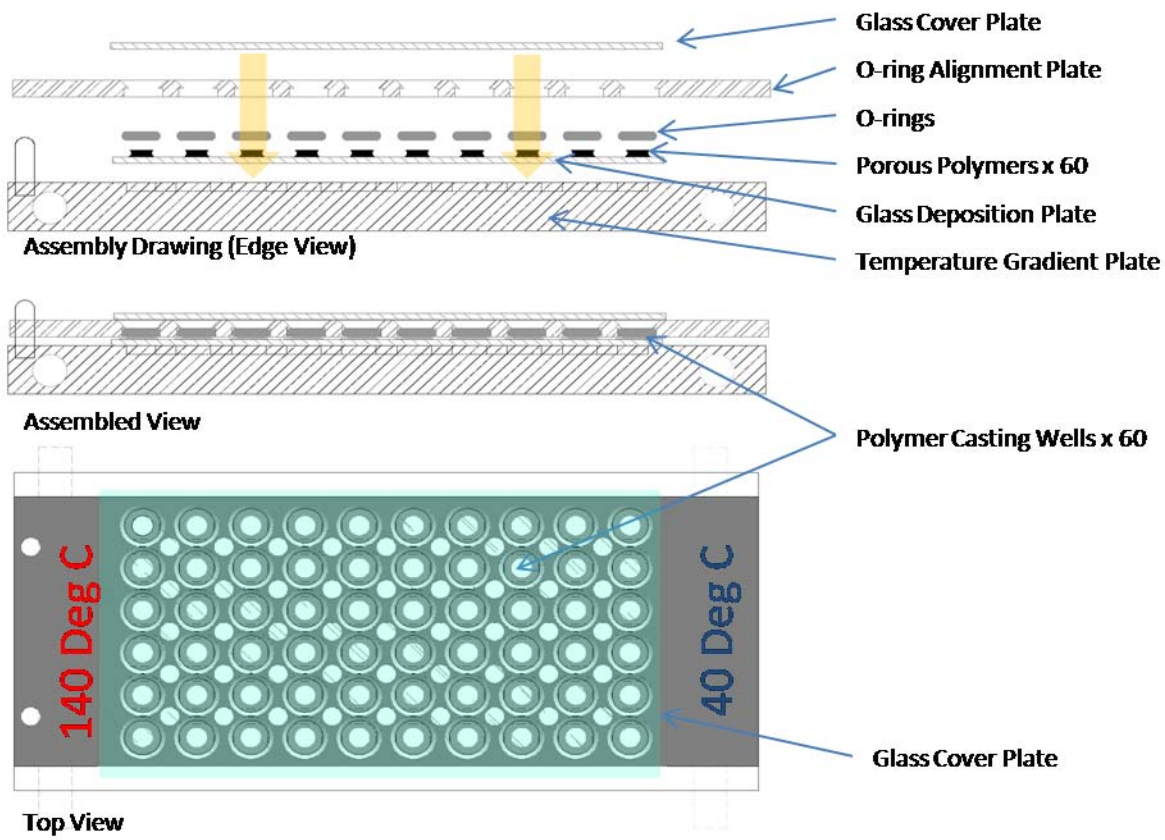

Figure 22. A schematic of the gradient plate design.

2.5. References

1. S. Salerno, M. Oliviero, E. Di Maio, S. Iannace, and P. Netti, "Controlled Preparation of Porous Scaffolds by Gas Foaming of Heterogeneous Blends," *AIP Conference Proceedings (IVth International Conference on Times of Polymers (TOP) and Composites)*, 1042, 102-104 (2008).
2. P. Vandezande, L. E. M. Gevers, J. Vermant, J. A. Martens, P. A. Jacobs, I. F. J. Vankelecom, "Solidification of Emulsified Polymer Solutions via Phase Inversion (SEPPI): A Generic Way To Prepare Polymers with Controlled Porosity," *Chem. Mater.*, 20, 3457-3465 (2008).
3. S. Eeltink, F. Svec, "Recent advances in the control of morphology and surface chemistry of porous polymer-based monolithic stationary phases and their application in CEC," *Electrophoresis*, 28, 137-147 (2007).
4. H. C. Silvis, K. J. Bouck, J. P. Godschalx, Q. J. Niu, M. J. Radler, T. M. Stokich, J. W. Lyons, B. J. Kern, J. G. Marshall, K. Syverud, and M. Leff, "Design of nanoporous polyarylene polymers for use as low - k dielectrics in microelectronic devices." *ACS Symposium Series (Polymers for Microelectronics and Nanoelectronics)*, 874, 187-198 (2004).

5. T. D. Li, L. M. Gan, C. H. Chew, W. K. Teo, and L. H. Gan, "Preparation of Ultrafiltration Membranes by Direct Microemulsion Polymerization Using Polymerizable Surfactants," *Langmuir*, 12, 5863-5868 (1996).
6. G. A. Lushcheikin, "New polymer-containing piezoelectric materials," *Physics of the Solid State*, 48(6), 1023-1025 (2006).
7. V. Vamvakaki and N. A. Chaniotakis, "Immobilization of Enzymes into Nanocavities for the Improvement of Biosensor Stability," *Biosensors & Bioelectronics*, 22(11), 2650-2655 (2007).
8. B. Adhikari and S. Majumdar, "Polymers in Sensor Applications," *Progress in Polymer Science*, 29(7), 699-766 (2004).
9. J. Germain, J. Hradil, J. M. J. Frechet, and F. Svec, "High Surface Area Nanoporous Polymers for Reversible Hydrogen Storage," *Chemistry of Materials*, 18(18), 4430-4435(2006).
10. J. Germain, F. Svec, and J. M. J. Frechet, "Preparation of Size-Selective Nanoporous Polymer Networks of Aromatic Rings: Potential Adsorbents for Hydrogen Storage," *Chemistry of Materials*, 20(22), 7069-7076 (2008).
11. H. Zhao, C. Jiang, X. He, J. Ren, and C. Wan, "Preparation of Micro-Porous Membrane Electrodes and Their Application in Preparing Anodes of Rechargeable Lithium Batteries." *Journal of Membrane Science*, 310, 1-6 (2008).
12. K. C. Khemani, Polymeric Foams: Science and Technology, American Chemical Society, Washington, DC, 1997.
13. N. R. Cameron, "High Internal Phase Emulsion Templating as a Route to Well-Defined Porous Polymers," *Polymer*, 46, 1439-1449 (2005).
14. H. Zhang and A. I. Cooper, "Synthesis and Applications of Emulsion-Templated Porous Materials," *Soft Matter*, 1, 107-113 (2005).
15. J. M. Torkelson and S. W. Song, "Coarsening effects on microstructure formation in isopycnic polymer solutions and membranes produced via thermally induced phase separation," *Macromolecules*, 27, 6389-6397 (1994).
16. J. Kiefer, J. L. Hedrick, and J. G. Hilborn, "Macroporous Thermosets by Chemically-Induced Phase Separation," *Adv. Polym. Sci.*, 147, 161-247 (1999).
17. J. S. Lee, A. Hirao, and S. Nakahama, "Polymerization of monomers containing functional silyl groups. 5. Synthesis of new porous membranes with functional groups," *Macromolecules*, 21, 274-276 (1988).
18. G. Wulff, "Enzyme-like Catalysis by Molecularly Imprinted Polymers," *Chem. Rev.*, 102, 1-27 (2002).
19. J. Kiefer, J. G. Hilborn, J. A. E. Manson, and Y. Leterrier, "Macroporous Epoxy Networks via Chemically Induced Phase Separation," *Macromolecules*, 29, 4158-4160 (1996).
20. J. P. Flory, Principles of Polymer Chemistry, Cornell University Press, Ithaca, 1953.
21. M. L. Huggins, "Theory of solution of high polymers," *J. Am. Chem. Soc.*, 64, 1712-1719 (1942).
22. P. Majumdar, E. Lee, N. Patel, K. Ward, S. J. Stafslien, J. Daniels, B. J. Chisholm, P. Boudjouk , M. E. Callow, J. A. Callow, and S. E. Thompson, "Combinatorial materials research applied to the development of new surface coatings IX: An investigation of novel antifouling/fouling-release coatings containing quaternary ammonium salt groups," *Biofouling*, 24(3), 185-200 (2008).

23. P. Majumdar, S. Stafslien, J. Daniels, and D. C. Webster, "High Throughput Combinatorial Characterization of Thermosetting Siloxane-Urethane Coatings Having Spontaneously Formed Microtopographical Surfaces," *J. Coat. Technol. Res.*, 4(2), 131-138 (2007).
24. A. Ekin and D. C. Webster, "Combinatorial and High-Throughput Screening of the Effect of Siloxane Composition on the Surface Properties of Crosslinked Siloxane-Polyurethane Coatings," *Journal of Combinatorial Chemistry*, 9(1), 178-188 (2007).
25. J. Brandrup, E. H. Immergut, and E. A. Grulke, Polymer Handbook (Fourth Edition, Volume 2), Wiley, New York, 1998.
26. http://www.fei.com/products/families/magellan-family.aspx

DISTRIBUTION

4 North Dakota State University
Attn: Bret J. Chisholm
1805 NDSU Research Park Drive
Fargo, ND 58102

1	MS0885	Justine E. Johannes	1810
1	MS0885	Richard J. Salzbrenner	1820
1	MS0886	James H. Aubert	1822
1	MS0887	Duane B. Dimos	1800
5	MS0888	Shawn M. Dirk	1821
1	MS0888	Patricia S. Sawyer	1821
1	MS1411	Mathias C. Celina	1821
2	MS9018	Central Technical Files	8944
2	MS0899	Technical Library	4536
1	MS0123	D. Chavez, LDRD Office	1011

Sandia National Laboratories